



**NUMERICAL MODELLING OF FORCED CONVECTION HEAT
TRANSFER IN AN OPEN CAVITY**

AHMET DENİZ

SEPTEMBER 2019

**NUMERICAL MODELLING OF FORCED CONVECTION HEAT
TRANSFER IN AN OPEN CAVITY**

**A THESIS SUBMITTED TO
THE GRADUATE SCHOOL OF NATURAL AND APPLIED
SCIENCES OF
ÇANKAYA UNIVERSITY**

**BY
AHMET DENİZ**

**IN PARTIAL FULFILLMENT OF THE REQUIREMENTS FOR THE
DEGREE OF
MASTER OF SCIENCE
IN
THE DEPARTMENT OF
MECHANICAL ENGINEERING**

SEPTEMBER2019

Title of the Thesis: **Numerical Modelling of Forced Convection Heat Transfer in an Open Cavity**

Submitted by **Ahmet DENİZ**

Approval of the Graduate School of Natural and Applied Sciences, Çankaya University.



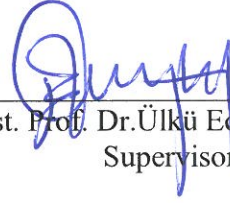
Prof. Dr. Can ÇOĞUN
Director

I certify that this thesis satisfies all the requirements as a thesis for the degree of Master of Science.



Prof. Dr. Haşmet TÜRKOĞLU
Head of Department

This is to certify that we have read this thesis and that in our opinion it is fully adequate, in scope and quality, as a thesis for the degree of Master of Science.



Assist. Prof. Dr. Ülkü Ece Ayli İNCE
Supervisor

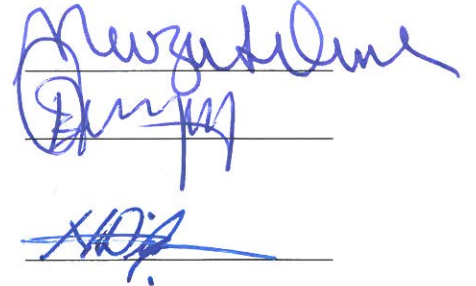
Examination Date:

Examining Committee Members

Prof. Dr. Nevzat Onur (Çankaya Univ.)

Assist. Prof. Dr. Ülkü Ece Ayli İnce
(Çankaya Univ.)

Assist. Prof. Dr. Nureddin Dinler (Gazi Univ.)



STATEMENT OF NON-PLAGIARISM PAGE

I hereby declare that all information in this document has been obtained and presented in accordance with academic rules and ethical conduct. I also declare that, as required by these rules and conduct, I have fully cited and referenced all material and results that are not original to this work.

Name, Last Name : Ahmet DENİZ

Signature : 

Date : 10.10.2019

ABSTRACT

NUMERICAL MODELLING OF FORCED CONVECTION HEAT TRANSFER IN AN OPEN CAVITY

DENİZ, Ahmet

M.Sc., Department of Mechanical Engineering

Supervisor: Dr. Ülkü Ece Ayli İNCE

July 2019, 71 pages

In this study, combined forced and natural convection heat transfer and fluid flow are examined in an open cavity. The effect of cavity geometries like cavity depth, cavity length, on heat transfer rate is investigated. As a flow parameter, Reynolds number, heat flux, heated wall position and Richardson number effect of the heat transfer are investigated.

The cavity left wall is heated with constant heat flux, while other walls are kept at the adiabatic condition. The working fluid is assumed as air with $Pr=0.71$. For numerical analysis FLUENT Software is used in order to solve incompressible, two-dimensional, steady-state flow. For momentum and energy equations second-order upwind scheme is used. Length to depth ratio and height to depth ratio of the cavity is varied between $0.25 < L/H < 5$, $0.25 < D/H < 3$, respectively. Reynolds number is changed between $24000 < Re < 96000$.

Keywords: Open cavity, mixed convection, inclined wall, heat transfer.

ÖZ

2 BOYUTTA AÇIK VE OYUKTA ZORLANMIŞ KONVEKSİYONUN NÜMERİK MODELLENMESİ

DENİZ, Ahmet

M.Sc., Makina Mühendisliği Bölümü

Danışman: Dr. Ülkü Ece Ayli İNCE

Haziran 2019, 71 Sayfa

Bu çalışmada, açık bir boşlukta doğal ve zorlanmış taşınım ısı transferi problem sayısal olarak incelenmiştir. Boşluk derinliği, boşluk uzunluğu, boşluk eğimi gibi boşluk geometrilerinin ısı transferi üzerindeki etkisi incelenmiştir. Akış parametresi olarak Reynolds sayısı, ısı akısı, ısıtılan duvar etkisi ve Richardson sayısının ısı transferine olan etkileri irdelenmiştir. Boşluk sol duvarı sabit ısı akısı ile ısıtılmış, diğer duvarlar adiyabatik durumda tutulmuştur. Çalışmada akışkan olarak hava kullanılmıştır ($Pr=0.71$). Sıkıştırılmaz, iki boyutlu, kararlı hal akışını çözmek için Fluent yazılımı kullanılmıştır. Kavite boy derinlik oranı ve kavite yükseklik derinlik oranı sırasıyla $0.25 < L/H < 5,0$ $0.25 < D/H < 3$ arasında değiştirilmiştir. Reynolds sayısı $24000 < Re < 96000$ arasında değiştirilmiştir.

Anahtar Kelimeler: Açık kavite, konveksiyon, eğimli duvar, ısı transferi

ACKNOWLEDGEMENTS

I want to express my sincere gratitude to Dr. Ülkü Ece Ayli İnce for her supervision, guidance, suggestions, and encouragement throughout the development of this thesis. I want to thank the thesis committee members for their advice and comments. I am grateful to Prof. Dr. Nevzat Onur for his inspiration and guidance.



TABLE OF CONTENTS

| | |
|--|-----|
| STATEMENT OF NON-PLAGIARISM PAGE | i |
| ABSTRACT | ii |
| ÖZ..... | iii |
| ACKNOWLEDGEMENTS..... | iv |
| TABLE OF CONTENTS | v |
| LIST OF FIGURES | vii |
| LIST OF ABBREVIATIONS | x |
| 1.INTRODUCTION | 1 |
| 2.DESCRPTION OF THE SOLUTION METHOD | 6 |
| 2.1 Navier-Stokes Equations | 6 |
| 2.2. Reynolds-Averaged Navier-Stokes Equations | 6 |
| 2.2.1. Boussinesq Approximation | 8 |
| 2.2.2. Turbulence Model | 9 |
| 2.2.2.1. k- ϵ Turbulence Model..... | 9 |
| 2.2.2.2. k- ω Turbulence Model..... | 10 |
| 2.3. Boundary Condition | 10 |
| 2.4. Problem Statement | 11 |
| 2.5. Post-Process..... | 14 |
| 2.6.Objectives of this study | 15 |
| 3.CRITICAL ANALYSIS OF NUMERICAL PARAMETERS EFFECT | 16 |
| 3.1. Mesh Independency Study | 17 |
| 3.2. Turbulence Model Study..... | 19 |
| 3.3. Comparison of 2-D and 3-D results | 20 |
| 3.4. Obtaining Hydrodynamically Developed Flow | 23 |
| 3.5. Validation with the Experimental Study | 25 |

| | |
|--|----|
| 4. THE EFFECT OF GEOMETRICAL PARAMETERS ON HEAT TRANSFER | |
| CHARACTERISTICS OF OPEN CAVITY | 28 |
| 4.1. D/H Effect on Heat Transfer Characteristics | 29 |
| 4.2. L/D Effect on Heat Transfer Characteristics | 32 |
| 5. EFFECT OF FLUID FLOW PROPERTIES PARAMETERS ON HEAT TRANSFER | |
| CHARACTERISTICS OF OPEN CAVITY | 35 |
| 5.1 Reynolds Number Effect on Heat Transfer Characteristics | 35 |
| 5.2. Heat Flux Effect on Heat Transfer Characteristics | 41 |
| 5.3. Effect of Heated Wall Position on Heat Transfer Characteristics | 44 |
| 5.4. Effect of Richardson Number on Heat Transfer Characteristics | 47 |
| 6. CONCLUSION | 49 |
| REFERENCES | 52 |

LIST OF FIGURES

| | |
|---|-----------|
| Figure 1. Four inlet and outlet configurations..... | 5 |
| Figure 2.1. Velocity components representation due to the RANS approach | 7 |
| Figure 2.2. Schematic view of the cavity and boundary conditions | 11 |
| Figure 2.3. Schematic view of the (a) base cavity geometry (b) heated wall | 12 |
| Figure 3.1. Mesh structure for case 3 | 18 |
| <i>Figure 3.3. Turbulence model study</i> | <i>19</i> |
| Figure 3.4. Schematic View of 2D and 3D computational domains..... | 20 |
| Figure 3.5. Temperature distribution for (a) $y=0$ m (b) $y=0.05$ m (c) $y=0.01$ m .. | 22 |
| Figure 3.6. Temperature difference for 2D and 3D analysis (case 1) | 22 |
| Figure 3.7 Velocity contour for channel flow (a) $Re=24000$ (b) $Re=48000$ (c) $Re=96000$ | 24 |
| Figure 3.8 Velocity distribution graphic for channel flow (a) $Re=24000$ (b) $Re=48000$ (c) $Re=96000$ | 25 |
| Figure 3.9. Validation of numerical model with experimental data | 26 |
| Figure 4.1. Numerical Cases | 28 |
| Figure 4.2 Temperature distribution for cavity with ratio of D/H | 29 |
| Figure 4.3. Averaged Nu number for cavity with ratio of D/H | 30 |
| Figure 4.4. Temperature contour and streamline for (a) $D/H=0.25$ (b) $D/H=1$ | 31 |
| (c) $D/H=2$ (d) $D/H=3$ | 31 |
| Figure 4.5. Temperature distribution for cavity with ratio of L/D | 32 |
| Figure 4.6. Velocity streamlines for (a) $L/D=0.25$ (b) $L/D=1$ (c) $L/D=2$ (d) $L/D=5$.. | 34 |
| Figure 5.1. Temperature distribution for cavity with Reynolds number..... | 36 |

| | |
|--|----|
| Figure 5.2. Velocity streamlines for (a)Re=24000 (b)Re=48000 (c)Re=96000 | 37 |
| Figure 5.3 Temperature contour for (a)Re=24000 (b)Re=48000 (c)Re=96000 | 39 |
| Figure 5.4. Nusselt number distribution versus Reynolds number | 40 |
| Figure 5.5. Temperature distribution for cavity with heat flux | 41 |
| Figure 5.6. Averaged Nu number for cavity with Heat Flux | 42 |
| Figure 5.7 Temperature contour for (a)100W/m ² (b) 200 W/m ² (c)300 W/m ² ... | 43 |
| Figure 5.8. Schematic view of the (a) assisting flow (b) opposing flow | 44 |
| (c) bottom heated flow | 44 |
| Figure 5.9. Temperature distribution for different heating locations | 45 |
| Figure 5.10. Nusselt number distribution for different heating locations | 45 |
| Figure 5.11. Temperature contour and velocity vector for (a) assisting flow | 46 |
| (b) opposing flow (c) bottom heated flow | 46 |
| Figure 5.12. Richardson number effect in the mixed convection of open cavity .. | 47 |
| Figure 6.1. Schematic view of open cavity with D/H<1 | 50 |
| Figure 6.2. Schematic view of open cavity with L/D>1 | 50 |

LIST OF TABLES

Table 2.1. Test cases matrix13

Table 3.1. Mesh Study Cases17

Table 3.2. Turbulence model error values19

Table 3.3. Experimental Test Cases26



LIST OF ABBREVIATIONS

CFD Computational Fluid Dynamics

NU Nusselt Number

Re Reynolds Number

T Temperature



LIST OF SYMBOLS

D height of the heated wall, m

g gravitational acceleration, $\mathbf{m/s^2}$

k thermal conductivity, W/mk

H height of the inflow and outflow openings, m

Nu average Nusselt number, $= \frac{q_c}{T_w - T_o} \frac{D}{k}$

q heat flux, $\mathbf{Wm^{-2}}$

Re Reynolds number, $= \mathbf{u_i H/v}$

T temperature, K

$\overline{T_w}$ average wall temperature, K

T_i ambient temperature

u_i inlet velocity, m/s

x horizontal coordinate distance, m

y vertical coordinate distance, m

Greek Symbols

β volumetric coefficient of expansion, K^{-1}

ϕ tube diameter, m

ν kinematic viscosity, m^2/s

θ maximum dimensionless wall temperature

ρ density, kgm^{-3}

Subscript

c convective

k conductive

i inflow

o ambient air

r radiative

w wall

Ω Ohmic dissipation

CHAPTER 1

INTRODUCTION

In many various engineering applications, heat transfer from open and inclined cavities have drawn a considerable amount of attention because of its importance. It has an extensive range of practice, so the mixed convection heat transfer in channels with open cavities has been examined widely. Especially in nuclear reactors, geothermal energy systems, heat exchangers and building air conditioning mixed convection flow in cavities are widely used. In the literature, several studies are affected in order to investigate the interaction of free stream flow-buoyancy flow inside the cavity both numerically and experimentally. The main aim of those studies is to enhance the heat transfer rate, provide the durability and reliability of the systems [1, 2].

Papanicolaou and Jaluria [3] examined the mixed convection transportation from an insulated heat source inside a rectangular enclosure numerically. It is shown that the average Nusselt number rises with the increase of the Richardson number at a constant Re number. In their other research, Papanicolaou and Jaluria [4,5], studied the mixed convection numerically in the case of an isolated, constant source of heat input within a rectangular enclosure. It is shown in the results that the heat transfer from source was a lot higher if the conductance of the solid wall was also higher.

Showole and Tarasuk [6] investigate the natural convection in inclined cavities numerically. They performed their analysis 2-dimensionally for incompressible, steady-state, viscous flow. They used k- ϵ turbulence model in order to solve the Reynolds stress term. They showed their results in the form of velocity and temperature profiles, and local and average heat transfer rates. Due to their results, inclination creates better mixing in the flow and causes higher heat transfer coefficient.

Polat and Bilgen [7], studied the steady-state laminar convection in two dimensions numerically where the side surface of the opening is heated with fixed heat flux. Due to their results, the angle of heated plate inclination affects the volumetric flow rate and heat transfer, so it is the finding that it is an important variable.

Bilgen and Oztop [8] examined the natural convection heat transfer numerically in the partially open and inclined square cavity, and this study shows that the inclination angle does not affect Nusselt number linearly. It is studied experimentally and numerically in the study of Ortiz et al. [9] that the turbulent natural convection in a tilted open cubic cavity with a vertical wall depended on prescribed heat flux. As a result, it shows that when the cavity of the system faces down, the average Nusselt number decreases along with inclination angle of that cavity. Opposite results are shown when the cavity is faced up. In the study of Mehrez et al. [10], it is observed that the inclination angle effects temperature distribution, flow field and heat transfer dominantly.

In an experimental study of Manca et al. [11], mixed convection in an open cavity with the heated wall is examined experimentally. The left wall of the cavity is heated while other walls are adiabatic. The flow and heat transfer within the cavity is controlled by Reynolds number, Richardson number, and the buoyancy parameter. The results were reported for Reynolds number between 100 and 1000. Richardson number is taken between 30-110 for Reynolds number 1000, and Richardson number is taken between 2800-8700 for Reynolds number 100. The rate of the length of cavity to the height of cavity (L/D) was taken in the range of 0.5-1.5. The range of the channel height to cavity height (H/D) was taken in the range of 0.5-1.0. It is found that the maximum dimensional temperature rise decreases when the Reynolds and Richardson number decreases. It is also found that for $Re=1000$ there were two different fluid motions which were a parallel forced flow and recirculation flow within the cavity. For $Re=100$ the buoyancy effects were stronger and determined the penetration of thermal starting from the plate wall (heated) into the upper channel.

In another experimental study, which was conducted by Cárdenas et al. [12] flow in square crossing is implemented to this study, the transient laminar opposing complex convection heat transfer from two symmetric open cubic cavities. The

openings are subjected to constant heat flux boundary condition, and the farther bounding walls of the cavities and the channel were adiabatic. The testings were done with various values of buoyancy strength, different Ri numbers from 32.17 to 300.77, different Reynolds number from 500 to 1500, fixed Prandtl number of $Pr = 7$ and different inclination $0 \leq \gamma \leq 360$ degrees each time. As a result of these number of experiments means temperature distributions and averaged Nu numbers were calculated. Results show that depending on the channel orientation and buoyancy strength, the temperature and flow acts with an oscillatory behavior and are not symmetric when the channel centerline considered. Addition to this it is found out that the Richardson number, heat transfer rates have been elucidating the strong 3-D structure of the flow.

A sequence of experimental studies is performed by Siddiqui, and Elatar [13-15] about turbulent flow patterns in channel flows of low Reynolds numbers of mixed convection with the use of PIV (Particle Image Velocimetry) method; also natural convection is heavy on forced convection in these studies. Wang et al. [16] worked convective heat transfer and buoyancy-influenced turbulent flow within a vertical platform passage when one wall is considered as adiabatic, and others were heated. Views of turbulent shear stress, velocity, turbulence production, and turbulence intensity are acquired from two-component LDA (laser Doppler anemometer) method. Kühn et al. [17] investigated large-scale flow patterns of turbulent convective airflow in lengthened rectangular convection cell with the use of large-scale PIV tomographic.

Recent improvement enhances the requirements of energy methods with greater dimension scale or more temperature difference, like about the food industry [18], building works [19], space applications [20], nuclear reactor [21], etc., where buoyancy force is stronger. Traditionally, the temperature and velocity fluctuations will occur, and the main features of heat transport can be altered when buoyancy variable is great [22, 23]. Zhang et al. [24] conducted large-scale water tests to work natural convection heat transfer in interior heated melt pool of reactor with large Rayleigh numbers maximal 10^{16} . The disparities of heat transfer are seen in the large Rayleigh segment and will increase even greater than enhancing Rayleigh numbers. Turbulent convection heat transfer from face at high-temperature differences and high length gauges (Gr is equal to, or less than 2.32×10^{12} and Re

is equal to or less than 8.9×10^5) had been investigated by Evans et al. [25] also a decline had been detected in heat transfer factor as Gr/Re^2 is enhanced up to 3.06 from 0.18.

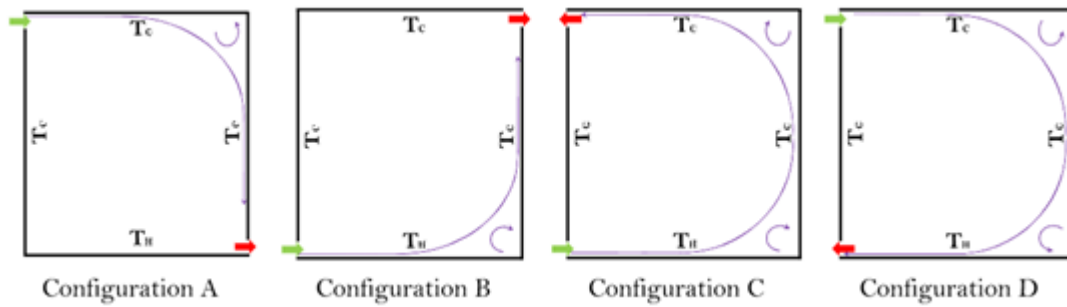
In a numerical study which was conducted by Burgos et al. [26], the unsteady and steady laminar flow in a channel with an open square cavity with heated bottom wall in 2-D is investigated. The Reynolds numbers were within 50-1000 and Richardson numbers were within 0.01-10. It is shown that the effect of the buoyancy force can be neglected when Richardson number is below 0.1. When Richardson number is 10 the buoyancy effect is significant and cannot be neglected. It is also observed that starting with $Re=500$ and $Ri=10$ the flow become unsteady.

In another numerical study which is conducted by Aminossadati and Ghasemi [27], the mixed convection heat transfer in a two-dimensional horizontal channel with an open cavity was numerically researched. There was a discrete heat source placed on one of the cavity walls. They changed the heat source location on each of their analyses (left, right, and bottom wall). The results have proven that there are recognizable differences between three heating types. When heat source was on the right wall the highest heat transfer rate is obtained when collated to other two types.

Rajarithnam et al. [28] have examined computationally Cu-nanofluid mixed convection inside a sloped fluid-saturated permeable cavity by taking into account three various states based on the direction of dynamic walls. By the help of Darcy-Brinkman-Forchheimer method, the nanofluid-saturated permeable medium equations are formed, and SIMPLE algorithm is used. The Darcy number, Richardson number, solid volume rate, inclination angle, and three various states as different dimensionless variables effects are examined. The acquired outcomes are offered as structure of isotherms, mean Nusselt number, streamlines, and mid-height velocity views.

Koufi et al. [29] have examined the heat transfer by mixed convection within ventilated cavities with exhaust and supply slots, and loaded with air under turbulent and constant flow regime numerically. Four different configurations are tried as it is given in Figure 1.

Figure 1. Four inlet and outlet configurations [adopted from [29]]



The lowest part of the cavity's temperature is held in T_H , and others are held in constant temperature as T_C . The cavity has two slots which are an outlet slot for extracting hot air and an inlet slot for letting in the fresh air. Due to their results, configuration D provides higher Nusselt number distribution when it is compared with the other configurations.

Timuralp and Altac [30], studied the heat transfer on open cavities with changing the cavity length and depth numerically. The front wall of the cavity is heated while for other walls adiabatic condition is utilized. Due to the results, increasing the depth of the cavity has a positive impact on heat transfer rates.

Manca et al. [31] studied the effect of a heated wall position in a cavity for $Re=100$ and 1000 . They also changed the cavity height to depth ratio in a range of $0.1-1.5$. According to their results for all of cases recirculating cells developed in the cavity. The highest Nusselt number is achieved in the opposing flow, and minimum thermal performance is obtained in the assisting flow.

CHAPTER 2

DESCRIPTION OF THE SOLUTION METHOD

In this study, mixed convection for turbulent flow regime in a cavity is investigated numerically. The left wall of the cavity is heated with constant heat flux, and other walls are assumed as adiabatic. A comprehensive investigation regarding to investigate the heat transfer rates in different cavity configurations, Reynolds numbers, and heat flux is performed with Computational Fluid Dynamics (CFD) techniques. For this purpose, ANSYS FLUENT [31] software is used. Finite Volume Method that solves the incompressible pressure-based Reynolds Averaged Navier-Stokes (RANS) equations is employed in order to solve this heat transfer problem. In this section, Navier-Stokes equations, employed boundary conditions, turbulence models that are used are given in detail. Also the effect of numerical parameters like turbulence model, mesh, 2D-3D effect is examined in this part. After obtaining a solution that is independent of numerical parameters verification study is performed with an experimental study.

2.1. Reynolds-Averaged Navier-Stokes Equations

Reynolds-Averaged Navier-Stokes (RANS) equations are Navier Stokes equations solved by turbulence models in turbulent flow analysis. In these equations, flow properties are divided into two components: time-averaged and time-varying parts as it is given in Figure 2.1. For example, the separation of speed quantities into components is as follows:

$$u_i = \bar{u}_i + u_i' \quad (2.1)$$

Here, \bar{u}_t represents the average of the velocity over time, and u'_t represents the difference in the amount of velocity concerning the average value.

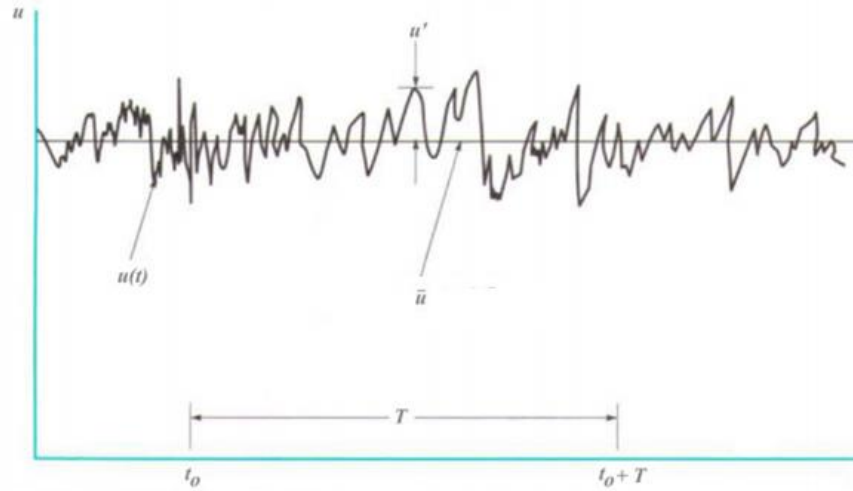


Figure 2.1. Velocity components representation due to the RANS approach

Other values, such as pressure, are expressed as components, such as velocity values. The Navier-Stokes equations are arranged using this principle, and the Reynolds Average Navier-Stokes (RANS) equations are obtained. Time-dependent RANS equations are called Reynolds-Averaged Navier-Stokes (URANS) equations. The continuity equation and URANS equations are given in Equation 2.2 - Equation 2.4 respectively.

(A) The motion of a viscous fluid conforming to Newton's law is defined by the Navier-Stokes equations. Navier-Stokes equations are the differential expressions of conservation of momentum of fluid in control volume. Governing equations of conservation of mass, momentum and energy will be given in Cartesian coordinates after making necessary assumptions and simplifications. In Cartesian coordinates, Navier-Stokes equations are expressed as follows:

Continuity

$$\frac{\partial \bar{u}}{\partial x} + \frac{\partial \bar{u}}{\partial y} = 0 \quad (2.2)$$

x-momentum

$$\rho \left(\bar{u} \frac{\partial \bar{u}}{\partial x} + \bar{v} \frac{\partial \bar{u}}{\partial y} \right) = -\frac{\partial \bar{p}}{\partial x} + \frac{\partial}{\partial x} \left(\mu \frac{\partial \bar{u}}{\partial x} - \rho \overline{u'u'} \right) + \frac{\partial}{\partial y} \left(\mu \frac{\partial \bar{u}}{\partial y} - \rho \overline{u'v'} \right) \quad (2.3)$$

y-momentum

$$\rho \left(\bar{u} \frac{\partial \bar{v}}{\partial x} + \bar{v} \frac{\partial \bar{v}}{\partial y} \right) = -\frac{\partial \bar{p}}{\partial y} + \frac{\partial}{\partial x} \left(\mu \frac{\partial \bar{v}}{\partial x} - \rho \overline{u'v'} \right) + \frac{\partial}{\partial y} \left(\mu \frac{\partial \bar{v}}{\partial y} - \rho \overline{v'v'} \right) \quad (2.4)$$

Energy

$$\rho c_p \left(\bar{u} \frac{\partial \bar{T}}{\partial x} + \bar{v} \frac{\partial \bar{T}}{\partial y} \right) = \left\{ \frac{\partial}{\partial x} \left[k \frac{\partial \bar{T}}{\partial x} - \rho c_p \overline{u'T'} \right] + \frac{\partial}{\partial y} \left[k \frac{\partial \bar{T}}{\partial y} - \rho c_p \overline{v'T'} \right] \right\} \quad (2.5)$$

Equations given above can be written in index notation as given below

$$\nabla \cdot (\vartheta(\rho E + p)) = \nabla \cdot \left(k_{eff} \nabla T - \sum_j h_j j_j + (\overline{\tau_{eff}} \cdot \vartheta) \right) + S_H \quad (2.5)$$

where k_{eff} is the effective conductivity ($k+k_t$, where k_t is the turbulent thermal conductivity, defined according to the turbulence model being used), and J_j is the diffusion flux of species j . The first three terms on the right-hand side of Equation 2.5 represent energy transfer due to conduction, species diffusion, and viscous dissipation, respectively. S_H includes the heat of chemical reaction, and any other volumetric heat sources you have defined.

Continuity equation

$$\frac{\partial}{\partial x_i} (\rho u_i) = 0 \quad (2.6)$$

Momentum equation

$$\frac{\partial}{\partial x_j} (\rho u_i u_j) = -\frac{\partial p}{\partial x_i} + \frac{\partial}{\partial x_j} \left[\mu \left(\frac{\partial u_i}{\partial x_j} + \frac{\partial u_j}{\partial x_i} - \frac{2}{3} \delta_{ij} \frac{\partial u_k}{\partial x_k} \right) \right] + \frac{\partial}{\partial x_j} (-\rho \overline{u'_i u'_j}) \quad (2.7)$$

2.2.1. Boussinesq Approximation

In the Reynolds-averaged approach, Reynolds stresses need to be well modeled. The relationship of Reynolds stresses to velocity gradients according to Boussinesq hypothesis is as follows:

$$-\rho \overline{u'_i u'_j} = \mu_i \left(\frac{\partial u_i}{\partial x_j} + \frac{\partial u_j}{\partial x_i} \right) - \frac{2}{3} \left(\rho k + \mu_t \frac{\partial u_k}{\partial x_k} \right) \delta_{ij} \quad (2.8)$$

2.2.2. Turbulence Model

The mathematical expression of turbulence is expressed by the Reynolds number, which is a dimensionless number with the rate of the inertial force of the fluid to the viscous force. The number of Reynolds depends on the density (ρ), velocity (U), viscosity (μ) of the fluid, and the characteristic length of the object in contact with the fluid.

Navier-Stokes equations cannot be solved analytically; therefore, assumptions are made to solve Navier-Stokes equations numerically. In the RANS modeling method, Navier-Stokes is converted to time-averaged equations as they are explained in the previous part. Taking the time average of the Navier-Stokes equations creates new unknowns like Reynolds stress term. To model, these term turbulence models are needed therefore turbulence modeling is the crucial issue in CFD simulations.

There is no exact turbulence model that can be used in all of the fluid dynamics and heat transfer problems. Therefore; several turbulence models are described in the literature. To find the appropriate turbulence model for the specific problem turbulence model study is performed and most accurate model is chosen due to this study. In this thesis, two-equation turbulence models are tried which are k- ϵ and k- ω turbulence models. Definitions of these turbulence models are given in detail below.

2.2.2.1. k- ϵ Turbulence Model

This model, which was finalized by Launder and Spalding [32], solves convection equations for turbulence kinetic energy and turbulence kinetic energy dissipation rate. Subduction (ϵ) for the unit mass is defined by the following correlation.

$$\epsilon = \mu \frac{\partial \bar{u}_i'}{\partial x_k} \frac{\partial \bar{u}_i'}{\partial x_k} \quad (2.9)$$

After making the necessary changes on this equation and adding the coefficients, the standard k-ε model equations take the following form.

$$\frac{\partial \rho k}{\partial t} + \frac{\partial \rho U_j k}{\partial x_j} = \tau_{ij} \frac{\partial u_i}{\partial x_j} - \rho \varepsilon + \frac{\partial}{\partial x_j} \left[(\mu + \sigma^* \mu_T) \frac{\partial k}{\partial x_j} \right] \quad (2.10)$$

2.2.2.2. k-ω Turbulence Model

The k-ω turbulence model, a two-equation model, was discovered by Kolmogorov [33] and developed over time. Kolmogorov defined the first turbulence parameter as turbulent kinetic energy (k) and the second parameter as the loss of unit turbulence kinetic energy (w). Kolmogorov made the mathematical definition of turbulence viscosity, turbulence length scale and subduction as $\mu_t = k/\omega$, $l = k^{1/2}/\omega$ and $\varepsilon = \omega k$. Kolmogorov obtained the following equation for turbulence loss. Turbulence kinetic energy equation (k) is given in Eq (2.11).

$$\frac{\partial k}{\partial t} + U_j \frac{\partial k}{\partial x_j} = \tau_{ij} \frac{\partial u_i}{\partial x_j} - \beta^* k \omega + \frac{\partial}{\partial x_j} \left[\left(\nu + \sigma^* \frac{k}{\omega} \right) \frac{\partial k}{\partial x_j} \right] \quad (2.11)$$

Specific dissipation rate equation is given below:

$$\frac{\partial \omega}{\partial t} + U_j \frac{\partial \omega}{\partial x_j} = \alpha \frac{\omega}{k} \tau_{ij} \frac{\partial u_i}{\partial x_j} - \beta \omega^2 + \frac{\sigma_d}{\omega} \frac{\partial k}{\partial x_j} \frac{\partial \omega}{\partial x_j} + \frac{\partial}{\partial x_j} \left[\left(\nu + \sigma \frac{k}{\omega} \right) \frac{\partial \omega}{\partial x_j} \right] \quad (2.12)$$

Closure Coefficients:

$$\alpha = \frac{13}{25}, \beta = \beta_0 f_b, \beta^* = \frac{9}{100}, \sigma = \frac{1}{2}, \sigma^* = \frac{3}{5} \quad (2.13)$$

2.3. Boundary Condition

Figure 2.1 shows the schematic view of the study. The cavity bottom and right wall are taken adiabatic while the right wall is heated with constant heat flux. The fluid enters the channel at the uniform velocity U_0 on the left and at a temperature of $T_0 = 300$ K. The upper wall of the free stream domain is considered as pressure far field. For the outlet, pressure outlet boundary condition is utilized.

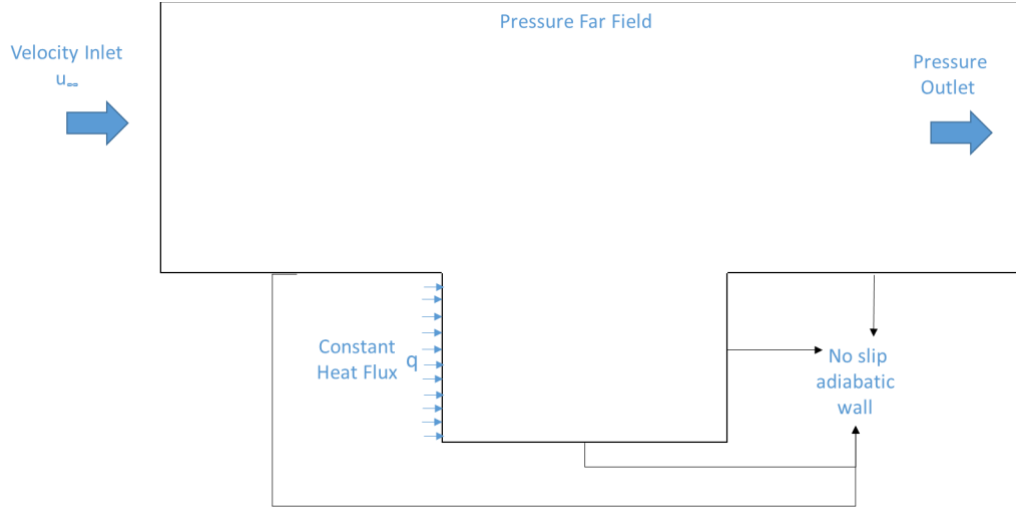


Figure 2.2. Schematic view of the cavity and boundary conditions

The utilized boundary conditions are summarized as follows:

$$\begin{aligned}
 u &= u_0, v = 0, T = T_0 \text{ at inlet} \\
 u' &= v' = 0, T' = 0 \text{ at duct outlet} \\
 \frac{\partial T}{\partial n} &= 0, u = v = 0 \text{ at adiabatic walls} \\
 k \frac{dT}{dy} \Big|_{y=D} &= q_w \text{ heated cavity wall}
 \end{aligned} \tag{2.13}$$

2.4. Problem Statement

Figure 2.3 indicates the schematic view of the study with the geometric parameters. The upper and lower walls were kept as adiabatic while the left wall is heated with constant heat flux. As working fluid water is used with $Pr=0.71$. Velocity value is varied for $Re=24000, 48000, 96000$. Flow is assumed as incompressible and two-dimensional. Since the flow is in a continuous regime, time-dependent terms are neglected. The test cases are given in Table 2.1. Channel L/D and D/H ratios are changed in order to investigate geometrical parameters effect on heat transfer. Also, heat flux and Reynolds number are changed to observe those parameters in Nusselt number. 33 different cases are analyzed to observe the effect of the geometrical parameters, Reynolds number, heat flux and heated wall effect.

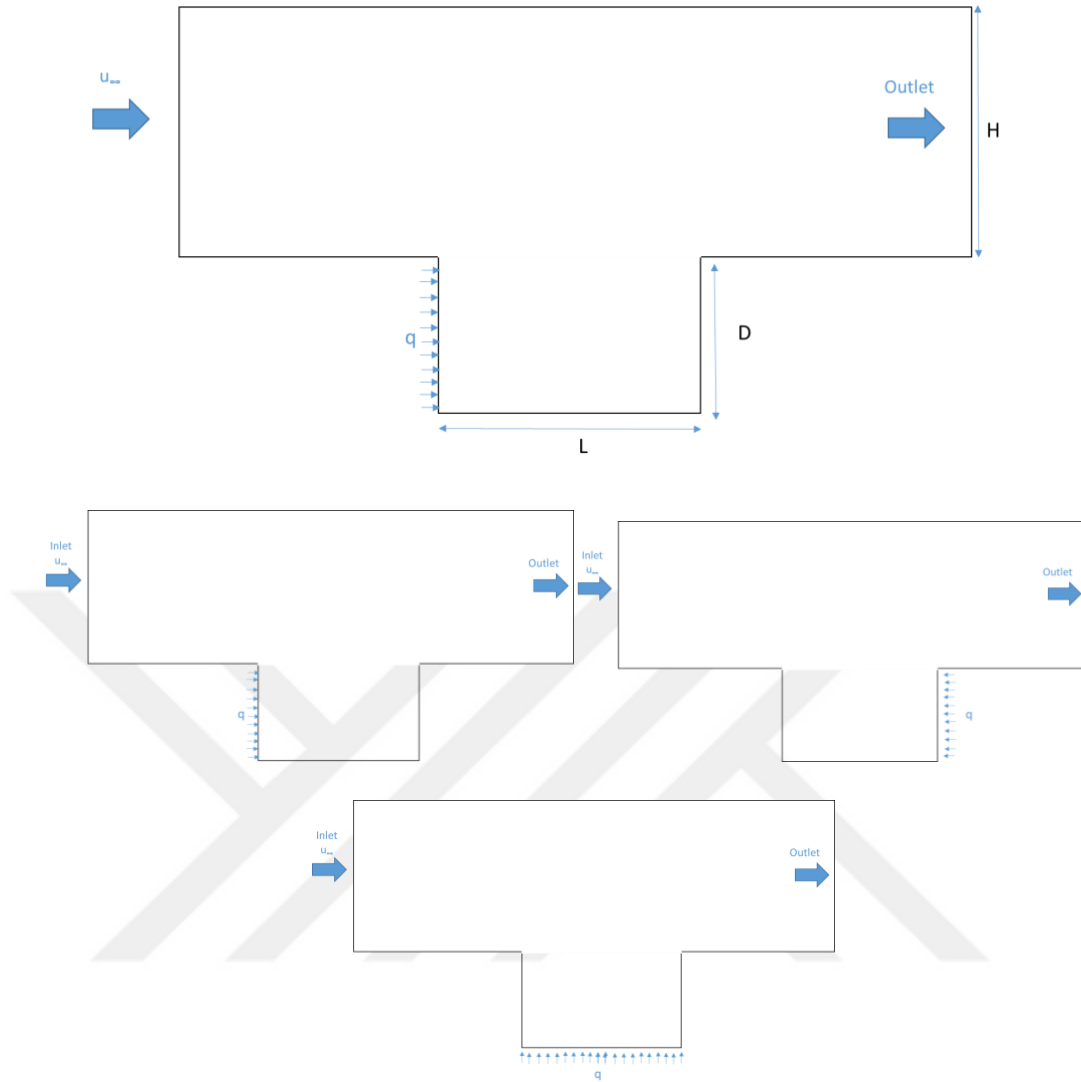


Figure 2.3. Schematic view of the (a) base cavity geometry (b) heated wall

In Figure 2.3, L denotes cavity length, D denotes cavity height, H denotes duct height. The ratio of cavity length to cavity height (L/H) is taken as 0.25, 1, 2 and 5; the ratio of duct height to cavity height (D/H) is taken as 0.25, 1, 2, 3. Reynolds number (Re) is taken as 24000; 48000 and 96000. Heat flux is taken as 100; 200 and 300 W/m^2 . To investigate the effect of the heating wall, opposing a wall, assisting wall and bottom wall is heated while other conditions are kept the same.

Table 2.1. Test cases matrix

| Test Case | L/H | H/D | Reynolds Number | Heated Wall | Heat Flux (W/m ²) | u _∞ (Free stream velocity) |
|-----------|------|------|-----------------|-------------|-------------------------------|---------------------------------------|
| 1 | 0.25 | 1 | 24000 | Left | 100 | 4.75 |
| 2 | 1 | 1 | | | | 4.75 |
| 3 | 2 | 1 | | | | 4.75 |
| 4 | 5 | 1 | | | | 4.75 |
| 5 | 1 | 0.25 | 24000 | | | 4.75 |
| 6 | 1 | 1 | | | | 4.75 |
| 7 | 1 | 1,5 | | | | 4.75 |
| 8 | 1 | 2 | | | | 4.75 |
| 9 | 1 | 3 | 48000 | | | 4.75 |
| 10 | 0.25 | 1 | | | | 9.54 |
| 11 | 1 | 1 | | | | 9.54 |
| 12 | 2 | 1 | | | | 9.54 |
| 13 | 5 | 1 | 48000 | | | 9.54 |
| 14 | 1 | 0.25 | | | | 9.54 |
| 15 | 1 | 1 | | | | 9.54 |
| 16 | 1 | 1.5 | | | | 9.54 |
| 17 | 1 | 2 | | | | 9.54 |
| 18 | 1 | 3 | 96000 | | | 9.54 |
| 19 | 0.25 | 1 | | | | 19.01 |
| 20 | 1 | 1 | | | | 19.01 |
| 21 | 2 | 1 | | | | 19.01 |
| 22 | 5 | 1 | 96000 | | | 19.01 |
| 23 | 1 | 0.25 | | | | 19.01 |
| 24 | 1 | 1 | | | | 19.01 |
| 25 | 1 | 1,5 | | | | 19.01 |
| 26 | 1 | 2 | | | | 19.01 |
| 27 | 1 | 3 | 19.01 | | | |

| | | | | | | |
|-----------|---|---|-------|--------|-----|-------|
| 28 | 1 | 1 | 48000 | | 100 | 9.54 |
| 29 | 1 | 1 | | | 200 | 9.54 |
| 30 | 1 | 1 | | | 300 | 9.54 |
| 31 | 1 | 1 | 96000 | Left | 100 | 19.01 |
| 32 | 1 | 1 | | Right | | 19.01 |
| 33 | 1 | 1 | | Bottom | | 19.01 |

2.5. Post-Process

Cavity flow which comprises the interaction of free stream flow and buoyancy flow inside the cavity, is solved numerically in the scope of the present thesis. In order to understand the flow physics, temperature contours, pressure contours, and velocity streamlines are used. To investigate the heat transfer characteristics Nusselt number is calculated for each case. The equations that are used are given below. The mathematical expression of turbulence is expressed by the Reynolds number which is a dimensionless number with the rate of the inertial force of the fluid to the viscous force. The number of Reynolds depends on the density (ρ), velocity (U), viscosity (μ) of the fluid, and the characteristic length of the object in contact with the fluid.

$$Re = \frac{\rho U D}{\mu} \quad (2.14)$$

Nusselt number is the rate of convective to conductive heat transfer at a boundary in a fluid. The Nusselt number is predicated on the difference between the wall and ambient temperatures. The mean Nusselt number is described in Equation (2.15).

$$Nu_{average} = \frac{h_{average} H}{k} = \frac{1}{A_H} \iint_{A_H} Nu dA \quad (2.15)$$

Where $h_{average}$ is the average heat transfer coefficient obtained from the relation that is given below:

$$h_{average} = \frac{q''}{T_w - T_\infty} \quad (2.16)$$

2.6. Objectives of this study

In this study, the numerical analysis will be performed for an open cavity under the mixed convection flow regime. The following researches are performed in the scope of the thesis.

- Verification of Numerical Model
- Mesh Independency Study
- Turbulence Model Study
- Dimension Effect
- The Effect of geometric parameters on mixed convection
 - ✓ L/D effect
 - ✓ H/D effect
- Heat flux effect
- Reynolds number effect
- Heated Wall Effect
- Richardson Number Effect

The results are reported in term of streamlines, velocity contours, temperature contours, temperature differences, and Nusselt number distributions.

CHAPTER 3

CRITICAL ANALYSIS OF NUMERICAL PARAMETERS EFFECT

In this part of the research, validation of the numerical model due to the experiment from the literature is performed. Also mesh independency and turbulence model is study is performed to be sure that obtained results are independent of the numerical parameters.

Numerical studies were carried out using Fluent Software [31], which is one of the computational fluids dynamics programs that analyze the main equations for fluid and heat transfer. For the present study, the Fluent [31] program analyzes the Re-averaged Navier-Stokes equations for the two-dimensional cavity flow with the infinite volume discretization approach. Pressure based Navier-Stokes equations are solved for incompressible, steady-state, viscous flow. Second degree Upwind method is used for discretization in the space, and the second-degree discretization method is used for discretization on time.

Results that are not independent of time and mesh structure are not very accurate in Computational Fluid Dynamics; therefore, time and mesh independency studies should be carried out and analysis should be started after minimizing numerical errors. In numerical studies, the selection of the appropriate turbulence model has a direct effect on flow physics, so the effects of various turbulence models on the flow must be examined. Also, 2D and 3D modeling effect on fluid behavior are investigated in this chapter.

This section describes the studies on the following topics.

- Mesh Independency Study
- Turbulence Model Study
- Dimension Effect
- Verification Study

3.1. Mesh Independency Study

To obtain accurate results which are not changing with increasing the number of mesh, mesh study is performed. The computational domain is meshed using structured grids which consist of quadrilateral elements. Mesh is tightened in the regions where the flow is critic and has a dominant effect on the performance. Element sizes for the meshes are given in Table 3.1.

Table 3.1. Mesh Study Cases

| | Mesh Type | Total Element |
|---------------|---------------|---------------|
| Case 1 | Quadrilateral | 150000 |
| Case 2 | Quadrilateral | 300000 |
| Case 3 | Quadrilateral | 600000 |
| Case 4 | Quadrilateral | 1000000 |

Mesh independency study is performed for, $Re=1000$ and $H=100$ mm with 50 W/m^2 heat flux value. In Figure 3.1, mesh structures are shown. In order to capture the complex flow structure in the region near the wall and shear layer the mesh has been well-controlled and refined at those zones. Due to Figure 3.2, after 6×10^5 element number mesh convergence is obtained. Therefore, with thinking the computational costs; case 3 is chosen as an appropriate mesh.

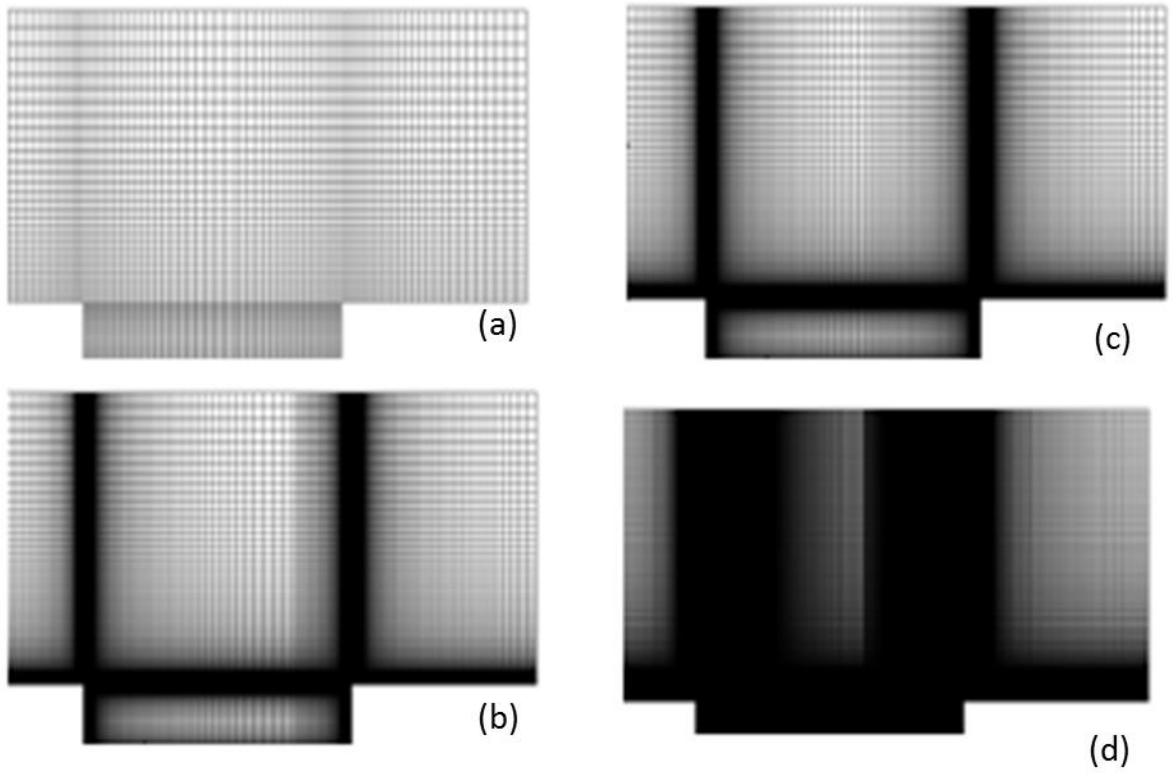


Figure 3.1. Mesh structure for case 3

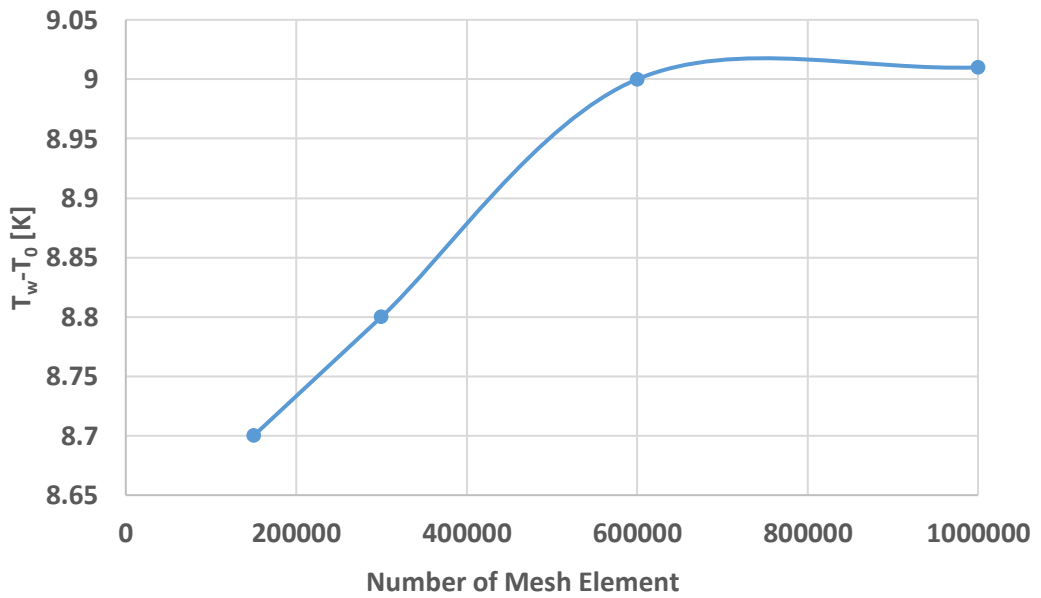


Figure 3.2. Wall temperature distribution for $y=50$ mm ($L/D=1$)

3.2. Turbulence Model Study

Turbulence model study is effected by comparing the temperature distributions for $L/D=1$, $Re=1000$, and 50 W/m^2 heat flux flow conditions. Figure 3.3 illustrates the temperature distributions that are obtained with three different turbulence models. All of the models' temperature distributions are compared with the experimental study that is performed by Manca et al. [11]. In Table 3.2, maximum errors are given for the turbulence models. Due to Figure 3.3. and Table 3.2, it is seen that $k-\omega$ SST turbulence model provides minimum error rates.

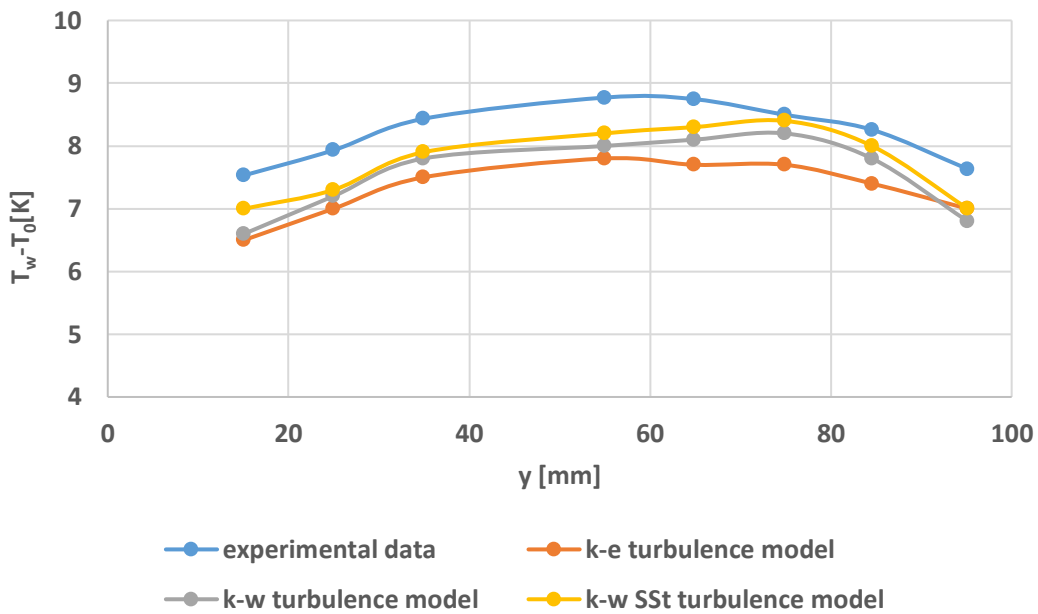


Figure 3.3. Turbulence model study

This model blends the $k-\omega$ and $k-\epsilon$ turbulence models and uses the advantages of both models. In the near-wall region $k-\omega$, in the free stream flow $k-\epsilon$ model is used. It is assumed that this model uses both of the model abilities, and it gives the most accurate results for this problem.

Table 3.2. Turbulence model error values

| Turbulence Models | RMSE (%) |
|-------------------|----------|
| $k-\epsilon$ | 7.529 |
| $k-\omega$ | 6.445 |
| $k-\omega$ SST | 5.058 |

3.3. Comparison of 2-D and 3-D results

In order to reduce the computational cost performing the 2-dimensional analysis is more time-efficient as it has fewer mesh elements. In Figure 3.4, schematical View of 2D and 3D computational domains are given for case 1.

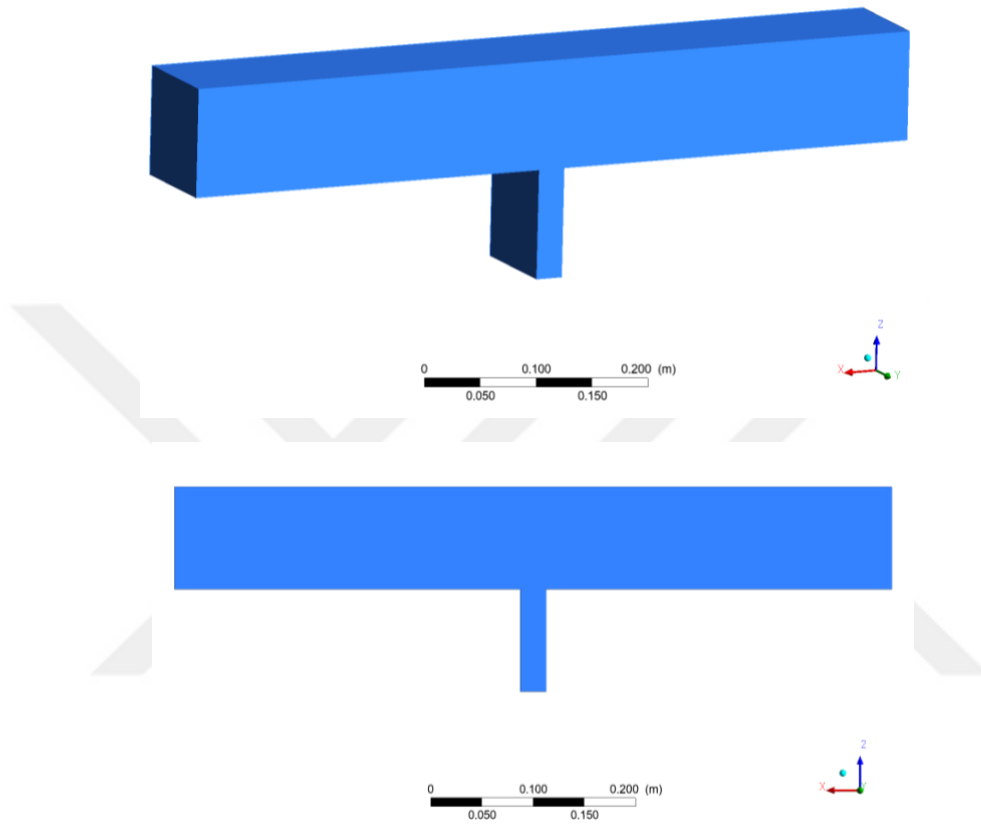


Figure 3.4. Schematic View of 2D and 3D computational domains

Before starting to investigate the effect of the geometrical and fluid flow parameters on mixed convection in a channel with an open cavity firstly 2-dimensional results are compared with 3-dimensional results for case 1 which has $L/D=0.25$, $D/H=1$, $Re=24000$, $q=100 \text{ W/m}^2$. To make accurate comparison firstly, for both 3D and 2D geometries meshes are refined until results are not varied with the mesh quality. It is the only way to make a comparison between 2D and 3 D simulations.

In Figure 3.5, temperature contours for 3-dimensional flow are shown for different planes. Although 3D simulations are more realistic and capture the gradients along the z-axis, in all of the planes flow behavior is similar to each other. This similar temperature flow distribution shows that there is a periodic behavior in the flow in the z-direction. Therefore making 2D analysis is enough to model the problem accurately.

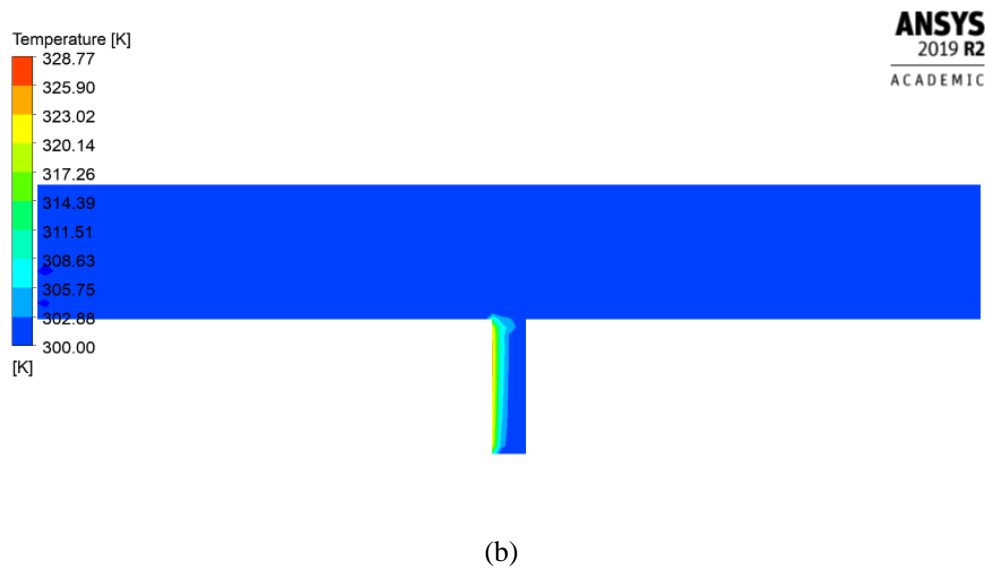
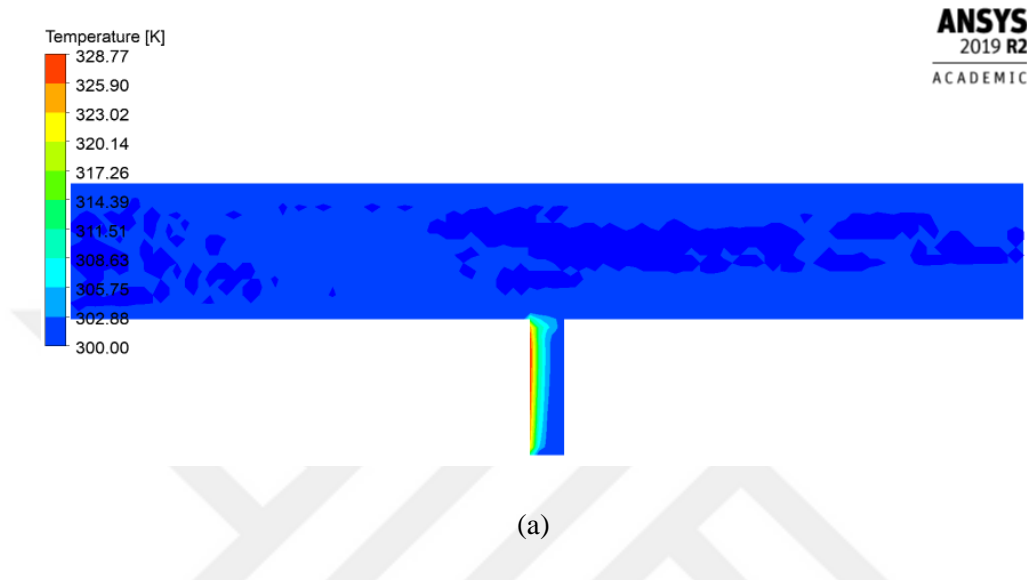
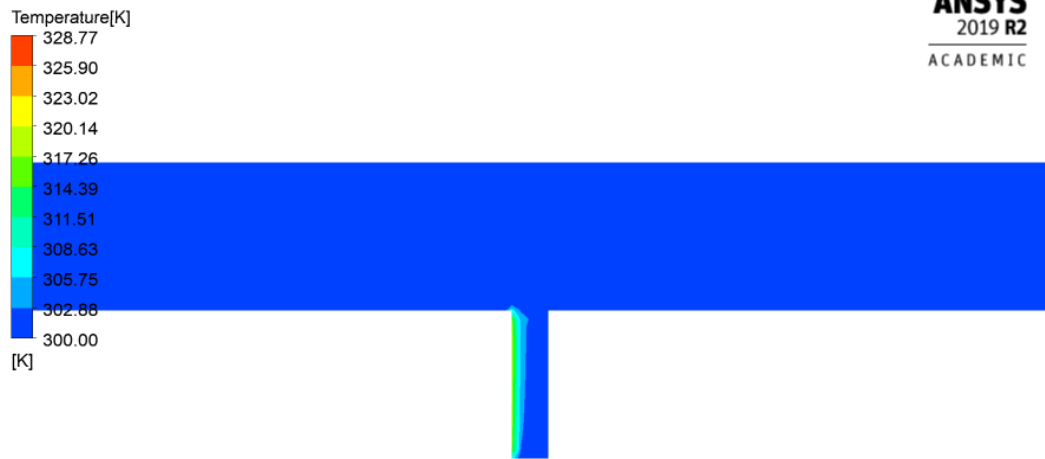


Figure 3.5. Temperature distribution for (a) $y=0$ m (b) $y=0.05$ m (c) $y=0.01$ m (cont.)



(c)

Figure 3.5. Temperature distribution for (a) $y=0$ m (b) $y=0.05$ m (c) $y=0.01$ m

In Figure 3.6. temperature difference that is obtained by making 2D and 3D analysis are shown. For both cases, temperature variation behavior is the same. The maximum difference between analysis is 2.3 %. This difference can arise because of the differing meshing procedures, boundary conditions and asymmetries which are unable to catch in a 2D domain. When computational costs are taken into account performing 2D approach will be enough to capture flow physics. Therefore, after this part of the study all of the analysis will be performed using 2D approach.

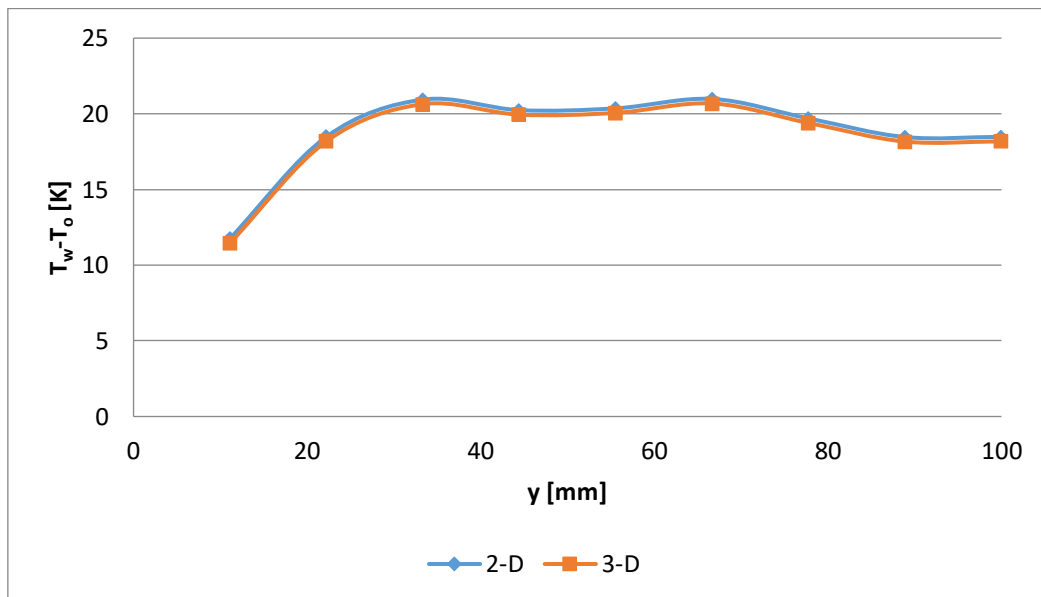


Figure 3.6. Temperature difference for 2D and 3D analysis (case 1)

3.4. Obtaining Hydrodynamically Developed Flow

When the viscous effects due to the shear stress between the fluid particles and pipe wall create a fully developed velocity profile it is known as fully developed flow. In order to reach a fully developed flow, 2-dimensional flow through a straight pipe is solved for all of the Reynolds numbers that are used in this study. In the inlet of the cavity, the obtained velocity profile is given, so flow is fully developed before entering the test section.

In Figure 3.7, the velocity profile is shown for different Reynolds numbers. It is seen that the velocity of the fluid at the wall is zero due to the shear stresses. As it is seen from the velocity contour, a boundary layer starts to form as the flow becomes developed. An inviscid core where shear stresses are negligible is formed in the channel.



(a)



(b)



(c)

Figure 3.7 Velocity contour for channel flow (a)Re=24000 (b)Re=48000 (c) Re=96000

In Figure 3.8, developed boundary layer profile is given for all of the Reynolds numbers. A parabolic shape velocity profile is obtained for all of the velocity values. The obtained fully developed velocity profile is given to the inlet of the cavity due to the reduced computational cost.

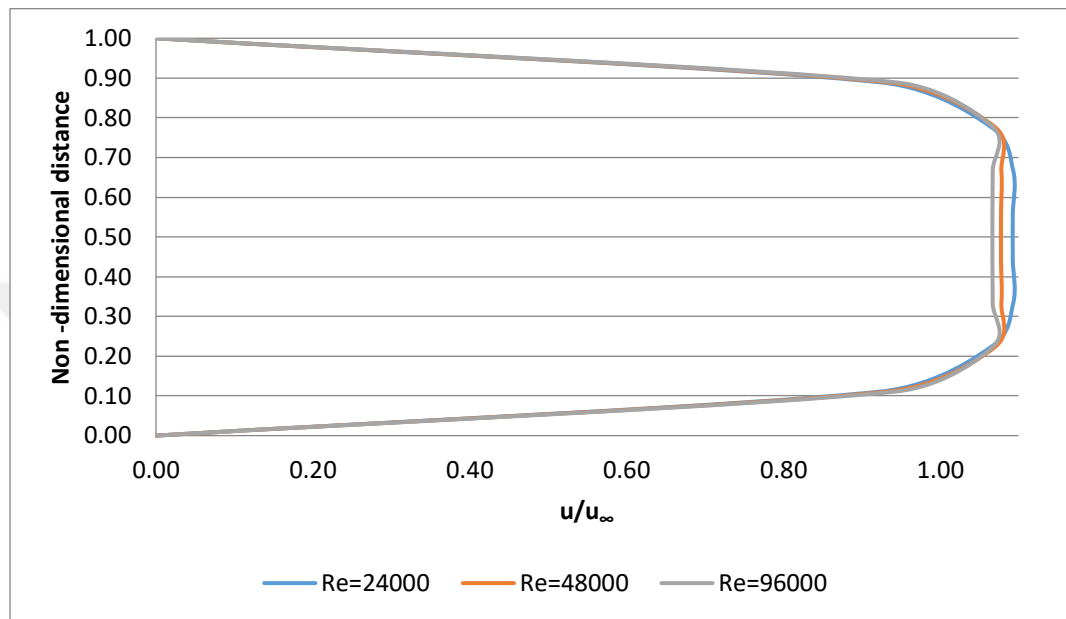


Figure 3.8 Velocity distribution graphic for channel flow

(a)Re=24000 (b)Re=48000 (c) Re=96000

3.5. Validation with the Experimental Study

Manca et al. [11] performed an experimental study for mixed convection in a channel with an open cavity. Experimental conditions are given in Table 3.3. Using the same conditions with experimental study, numerical analysis is conducted, and results are compared with each other using the temperature distribution. For two different experimental geometrical configurations validation is performed in the first case $H/D=1$ and the second case $H/D=0.5$.

Table 3.3. Experimental Test Cases

| | Case 1 | Case 2 |
|------------------------------------|--------|--------|
| Reynolds Number | 1000 | 1000 |
| Heat Flux (W/m²) | 100 | 100 |
| L/D | 0.5 | 2 |
| H/D | 1 | 0.5 |

To check the accuracy of the numerical method and calculations used in the present study, the results obtained were collated with Manca et al [11]’s study. Figure 3.4 indicates the results of the numerical study. Due to the comparison between numerical and experimental study maximum error is 6.8 %. Temperature distribution trend is observed similar to the experiment and in the numerical study. It is seen that in the middle of the cavity temperature difference reach its maximum value for both in the numerical and experimental study. When L/D ratio increases wall temperature decreases as it is seen from Figure 3.4.

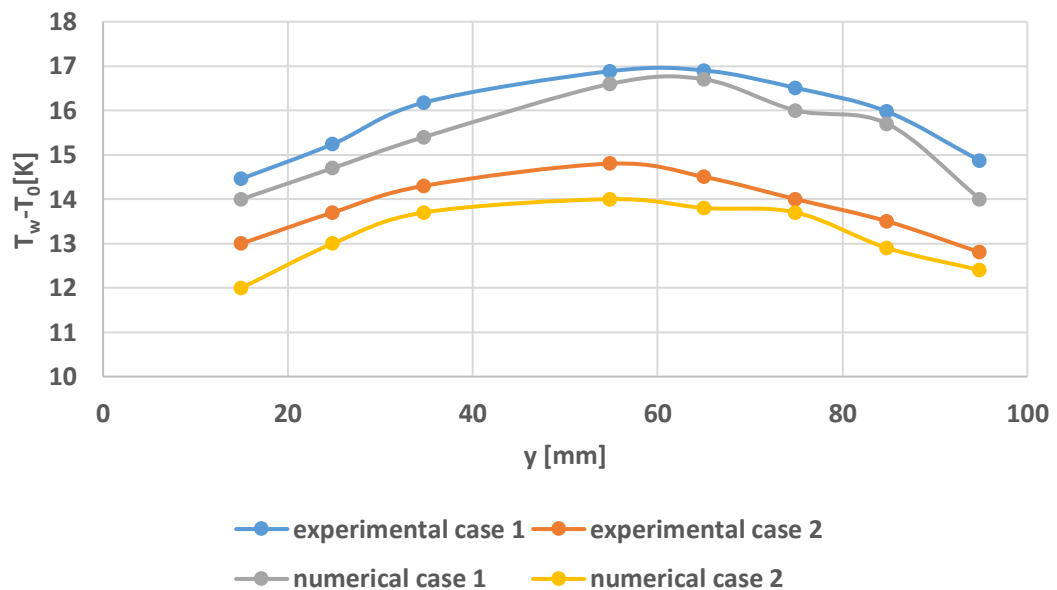


Figure 3.9. Validation of a numerical model with experimental data [11]

This part gives brief information about the effect of numerical parameters in the flow. As the accuracy of the results is limited by the available computer power, 2D approach is selected. The maximum difference between 2D and 3D approach is 2.3 %. To obtain hydrodynamically fully developed flow cavity entrance length should be ten times of the

cavity length. However, this entrance length will increase the computational cost. Therefore, a fully developed velocity profile is obtained with performing a duct flow analysis and obtained profile is used as an inlet in the cavity flow. This is the second approach that will decrease the computational cost. Also in this part mesh independency study and turbulence model study are performed. After developing a methodology that is independent of numerical parameters, the effect of geometrical parameters on mixed convection in an open cavity is investigated in the following part.



CHAPTER 4

THE EFFECT OF GEOMETRICAL PARAMETERS ON HEAT TRANSFER CHARACTERISTICS OF OPEN CAVITY

The numerical cases that are investigated are given in Figure 4.1. The scope of this part investigates the geometrical parameters effect on heat transfer flow in a cavity. In this part of the thesis, results will be given as given below:

- L/D effect: D/H is kept 1 for all of the cases and L/D ratio is changed between 0.25 to 5.
- D/H effect: L/D is kept 1 for all of the cases, and the D/H ratio is changed between 0.25 to 3.

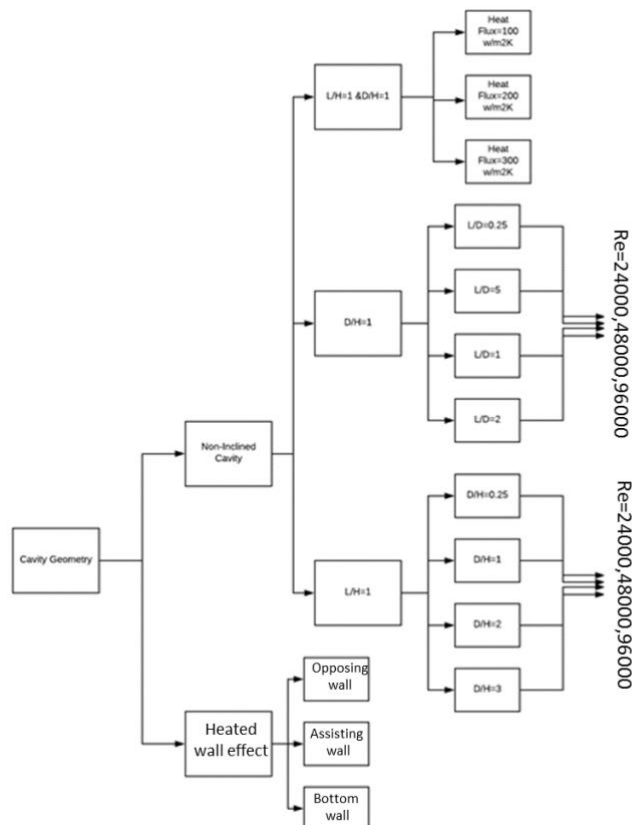


Figure 4.1. Numerical Cases

4.1. D/H Effect on Heat Transfer Characteristics

In order to examine the effect of cavity depth effect on the flow topology and heat transfer phenomena, D / H ratio is taken as 0.25,1,1.5, 2 and 3. The temperature distributions and temperature contours are obtained for all of the H/D ratios for Reynolds number 800 and heat flux $100\text{w} / \text{m}$ are given as follows.

In Figure 4.2, the temperature distribution for different ratio of D/H is illustrated. For all of the cases all the other parameters are kept constant as $L / D = 1$, $Re=800$ and 100 w/m^2 heat flux value. As it is depicted in Figure 4.3, decreasing D/H ratio which means increasing the cavity depth rises the temperature difference. It can be concluded that increasing the cavity depth causes lower heat transfer coefficient and heat transfer characteristics.

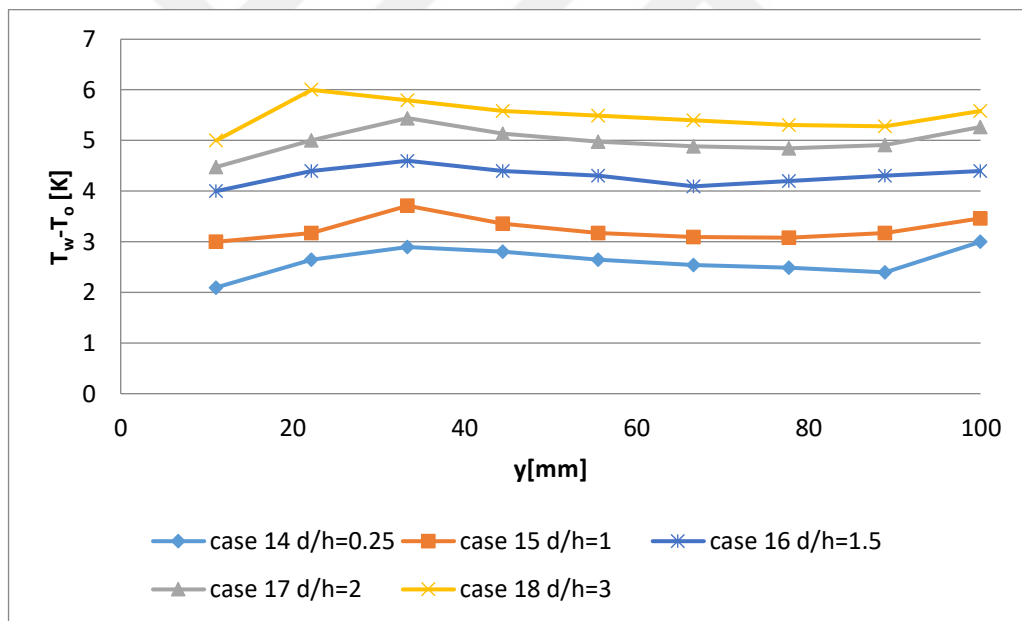


Figure 4.2 Temperature distribution for a cavity with a ratio of D/H

As it is given in Figure 4.3, the maximum temperature difference means minimum Nusselt number. Also it is seen that the trend of the temperature difference distribution and Nusselt number distribution are similar. This situation can also be observed from the mathematical formulation of the Nusselt number. Due to the obtained Nusselt number distribution, minimum D/H ratio causes maximum Nusselt number.

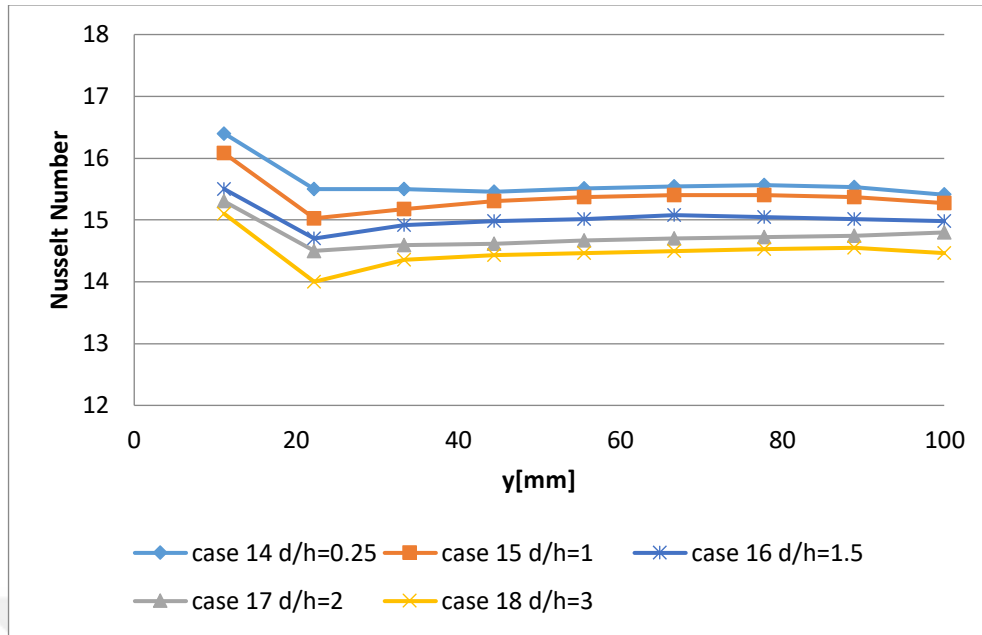


Figure 4.3. Averaged Nusselt number for a cavity with a ratio of D/H

In Figure 4.4, temperature contours and streamlines in the cavity zone are depicted for different cavity depths. Due to the contours, a vortex structure is observed in the cavity region. When the cavity depth is smaller or equal to the cavity height, vortex structure fills the cavity zone and reach to the bottom wall of the cavity. When the vortex structure is large, turbulence kinetic energy is also high in the cavity region which causes higher Nusselt number distribution. When depth value is larger than the height ($D/H > 1$), vortex structure can not reach to the bottom wall, and incoming air can not penetrate to the bottom wall. As incoming and warm air mixing is lower in the $D/H > 1$ configuration Nusselt number is smaller when it is compared with the $D/H < 1$ configuration.

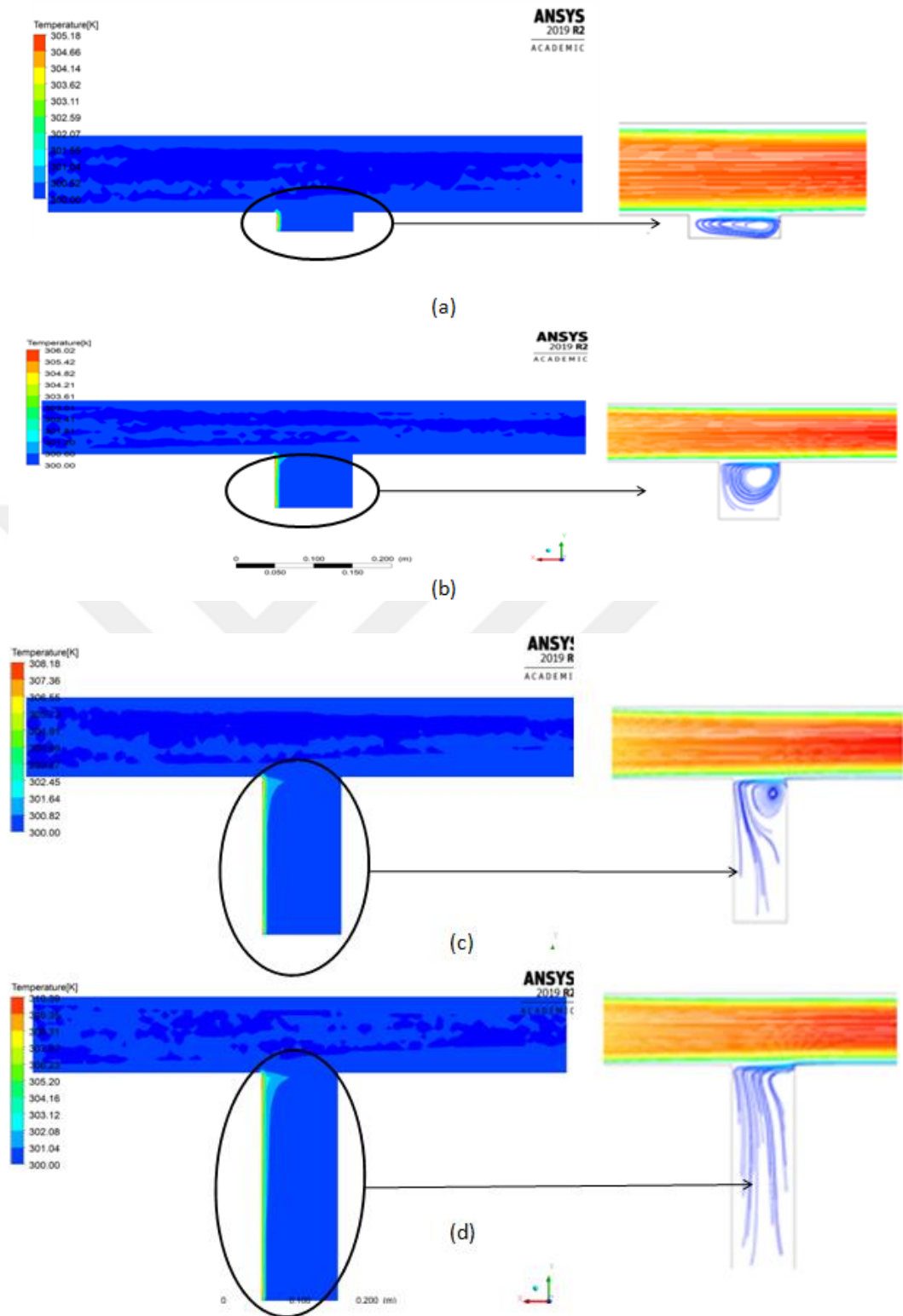


Figure 4.4. Temperature contour and streamline for (a) $D/H=0.25$ (b) $D/H=1$
(c) $D/H=2$ (d) $D/H=3$

4.2.L/D Effect on Heat Transfer Characteristics

In order to examine the effect of channel length on the flow, L/D ratio is changed as 0.25,1,2,5. Reynolds number is 48000 and heat flux is 100 W/m^2 for all of the cases. Figure 4.5 shows that as the L/H ratio increases the temperature difference decreases.

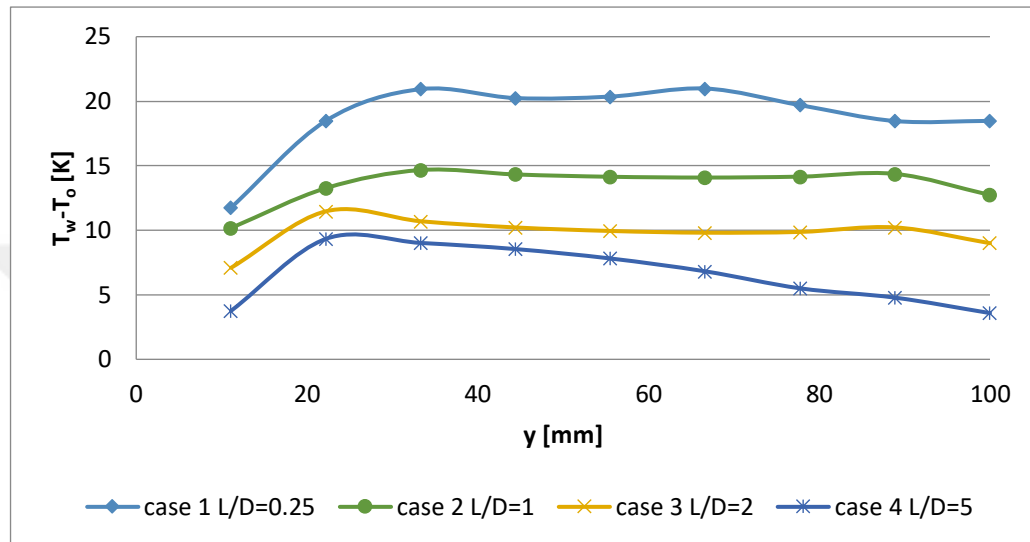


Figure 4.5. Temperature distribution for a cavity with ratio of L/D

Vortex structures increase the turbulent effect which causes reduction in the temperature values. Figure 4.6 shows that when the L / H ratio is 0.25, no vortex occurs in the cavity region because the cavity is narrow. As incoming air cannot mix with the fresh air efficiently, Nusselt number is higher in the narrow cavity configuration. When cavity length increases vorticity is formed in the cavity region. When L/D=1, vortex structures filled the 88% of the cavity volume which means turbulence is created in the cavity zone. When L/D ratio is increased to 2, secondary vortex region is occurred in the left wall of the cavity. At L/D=5, three vortex structures observed in the cavity which means the highest turbulent is generated in the maximum length. Therefore, it can be concluded increasing the cavity length, increases the turbulent effect which causes heat transfer enhancement with higher Nusselt number values.

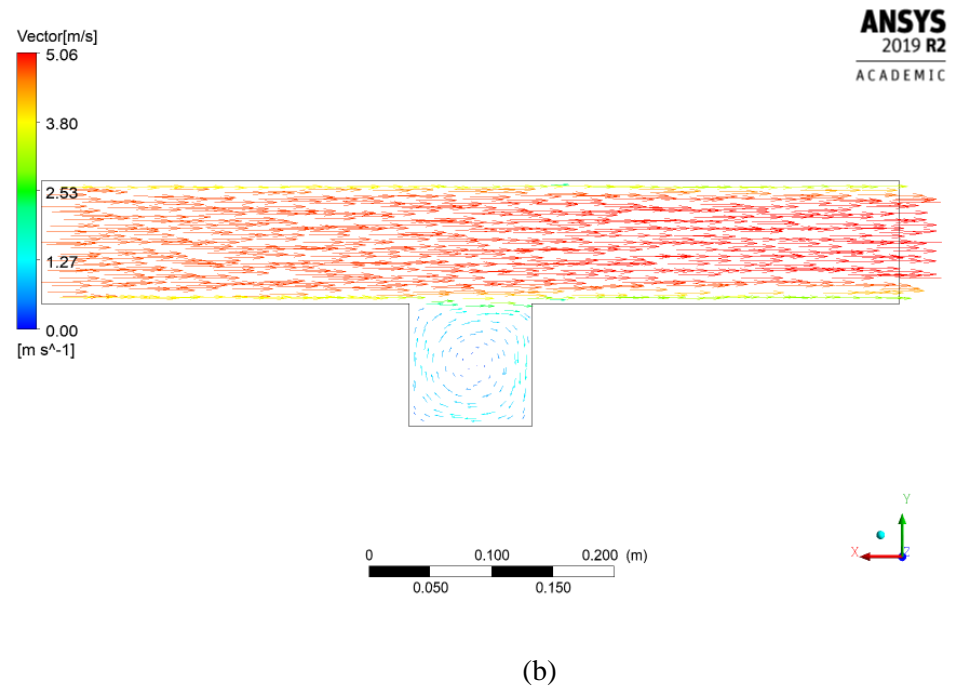
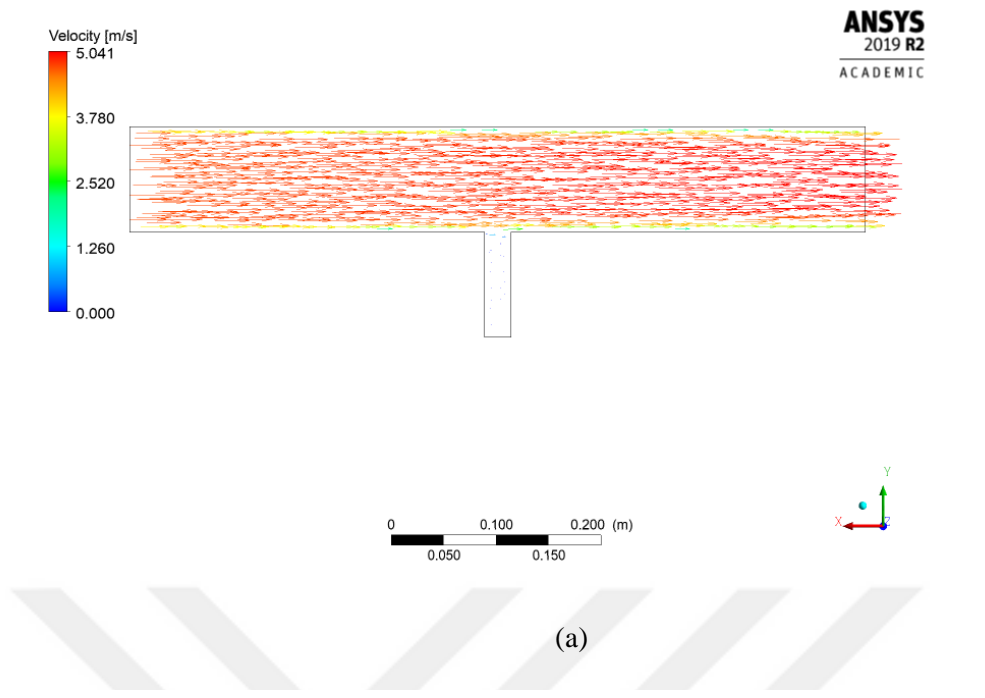


Figure 4.6. Velocity streamlines for (a) $L/D=0.25$ (b) $L/D=1$ (c) $L/D=2$ (d) $L/D=5$ (cont.)

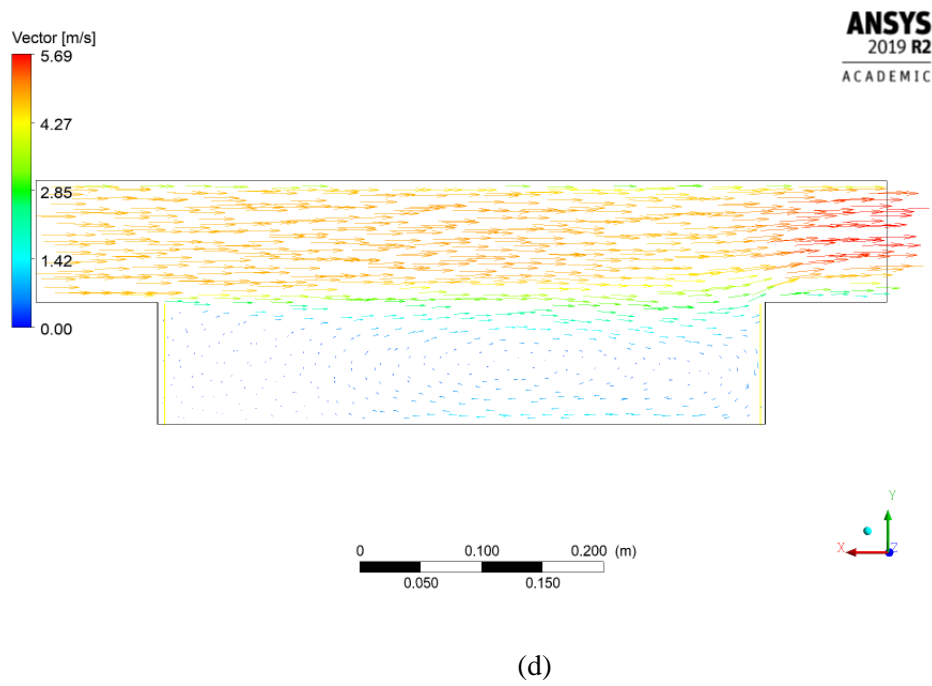
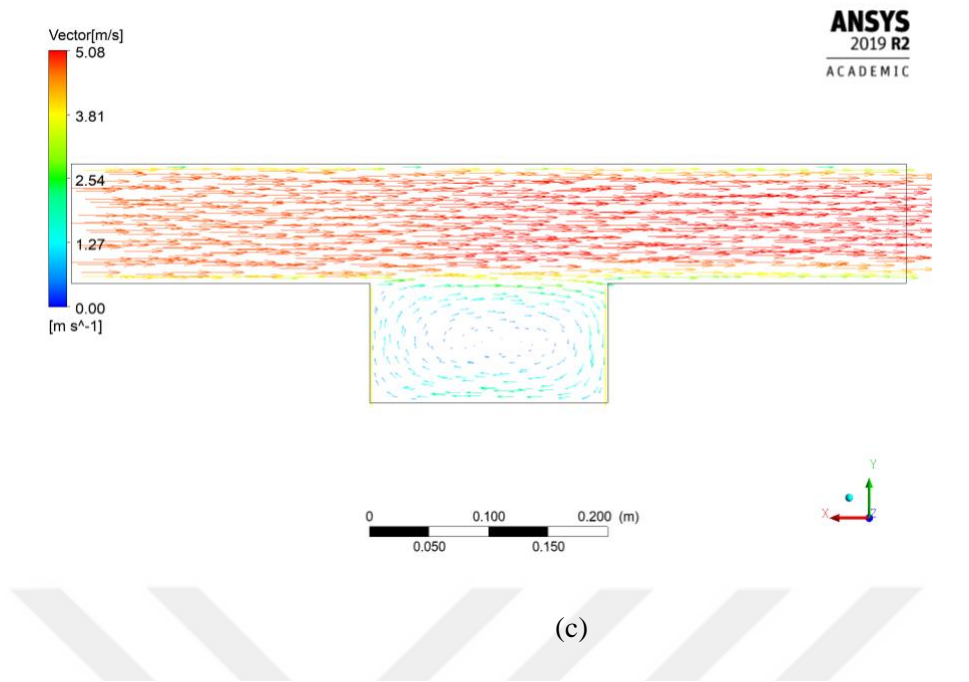


Figure 4.6. Velocity streamlines for (a) $L/D=0.25$ (b) $L/D=1$ (c) $L/D=2$ (d) $L/D=5$

CHAPTER 5

EFFECT OF FLUID FLOW PROPERTIES PARAMETERS ON HEAT TRANSFER CHARACTERISTICS OF OPEN CAVITY

In this chapter, combined convection cavity-channel domain is studied numerically for different Reynolds numbers and heat flux values. Also, the effect of heated wall position in a channel is examined. Three basic heating modes are considered as (a) the heated wall is in the leading side (called as assisting flow) (b) heated wall in the trailing edge side (called as opposing flow) (c) heating from the bottom wall. The results are reported in terms of contours, vectors, temperature distribution, and Nusselt number distribution.

5.1 Reynolds Number Effect on Heat Transfer Characteristics

Reynolds number; is the rate of a fluid to viscosity forces of inertia forces. In the present study, the Re number is only affected by the velocity parameter since the density and viscosity are kept constant. The effect of velocity on flow and temperature was examined by taking Reynolds number 24000, 48000, 96000.

In Figure 5.1, the temperature distribution for different Reynolds number is illustrated. For all of the cases all the other parameters are reserved constant in $L / D = 1$, $D / H = 1$ and $100 \text{ w} / \text{m}^2$ heat flux value. As it is depicted in Figure 5.1, increasing the Reynolds number decreases the temperature difference which means that better heat transfer characteristics with higher Nu number. For all of the cases, maximum temperature is obtained nearly in the middle of the wall.

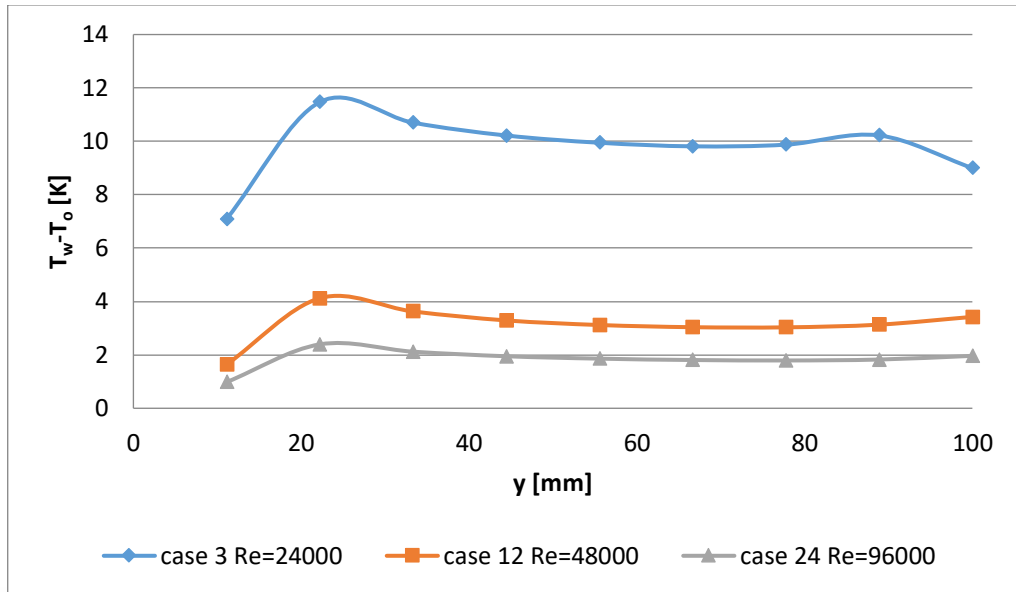
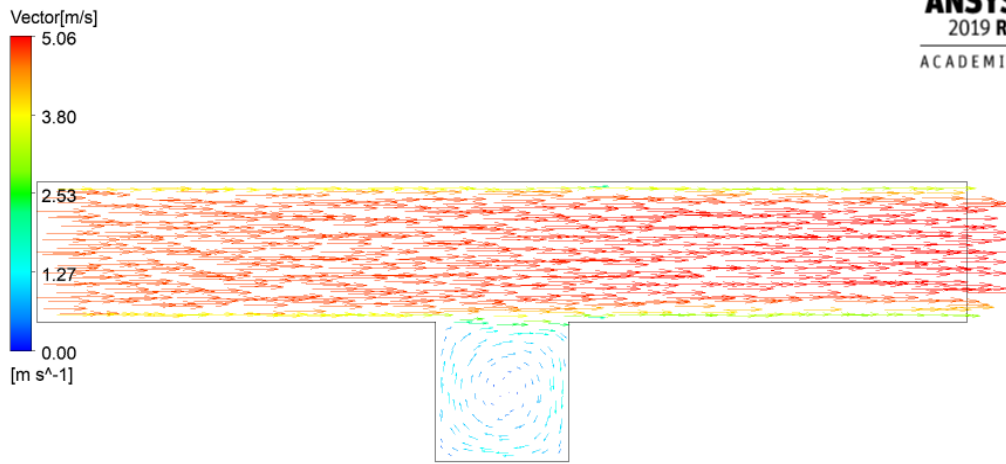
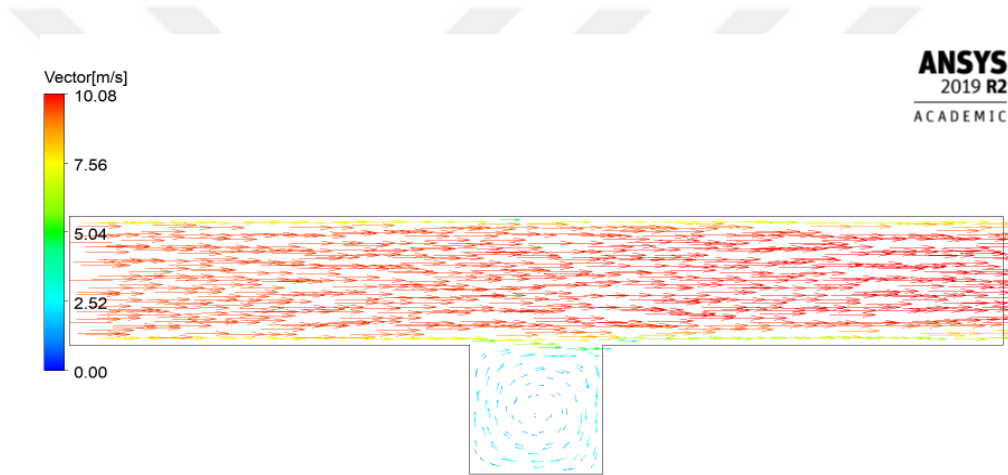


Figure 5.1. Temperature distribution for a cavity with Reynolds number

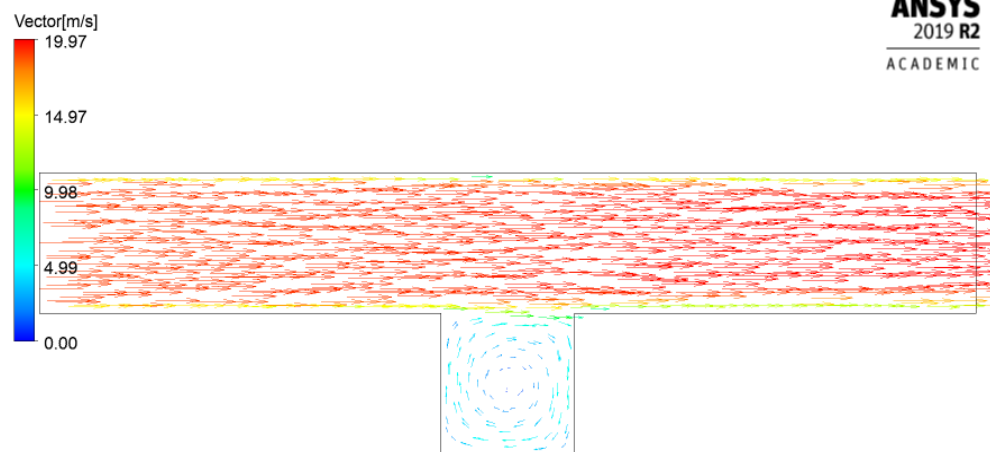
As the geometrical properties are kept the same for all the cases, the temperature distribution trend is observed similarly. This situation is also depicted with streamlines as it is given in Figure 5.2.



(a)



(b)



(c)

Figure 5.2. Velocity streamlines for (a)Re=24000 (b)Re=48000 (c)Re=96000

In the cavity zone, a vortex structure is observed for all of the cases. Almost 83% of the cavity volume filled with the vortex structure. Although the flow topology is same for all of the cases velocity values increased with rising the Reynolds number. In Figure 5.2(c) as Reynolds number is reached to the highest value, free stream velocity value also reached to its maximum value which causes more forced convection effect on the cavity zone. Therefore, Nusselt number and heat transfer coefficient are the highest when $Re=1600$.

In conclusion, it is found that Reynolds number has a proportional relationship with the Nusselt number which means increasing the Reynolds number creates more turbulence and increases heat transfer rates.

In Figure 5.3, temperature contour is shown for open cavity with different Reynolds numbers. It is seen that flow regime is almost same for whole cases on the other hand as Reynolds number is varied, maximum temperature changes due to the velocity variation.

When Reynolds number is 24000, the maximum temperature reaches to the 312 K, when Reynolds number increased to the 96000, maximum temperature drops to 303 K. Temperature distribution trend is observed same for three cases, but maximum temperature value changes. According to the results; temperature decreases when Reynolds number increases. The reason for this situation is increasing the Reynolds number rises the kinetic energy inside the cavity. Also the cold air penetrates to the warm air better when Reynolds number increases.



(a)



(b)



(c)

Figure 5.3 Temperature contour for (a)Re=24000 (b)Re=48000 (c)Re=96000

As the Reynolds number is one of the most crucial parameters in the flow field in Figure 5.4, average Nusselt number distribution for different Reynolds number is depicted. With increasing the Reynolds number, the heat transfer coefficient and Nusselt number rises which means better heat transfer enhancement.

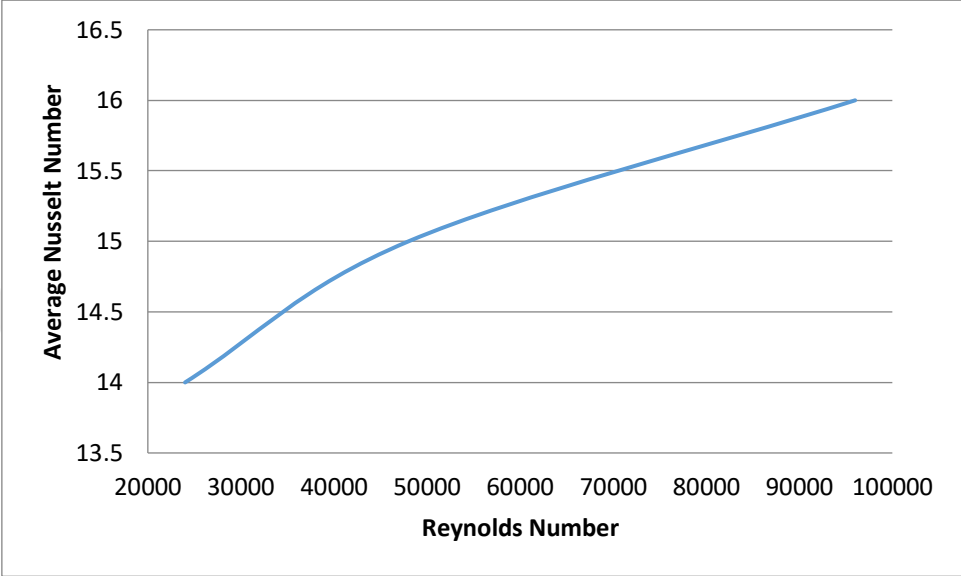


Figure 5.4. Nusselt number distribution versus Reynolds number

5.2. Heat Flux Effect on Heat Transfer Characteristics

Heat energy passing through the unit area is called heat flux. In order to observe the heat flux effect, geometry and Reynolds Number were kept constant, and heat flux values were changed to 100,200 and 300 W/m². As it is given in Figure 5.5, the temperature difference increases with increasing the heat flux value which means that heat flux and temperature difference are directly proportional.

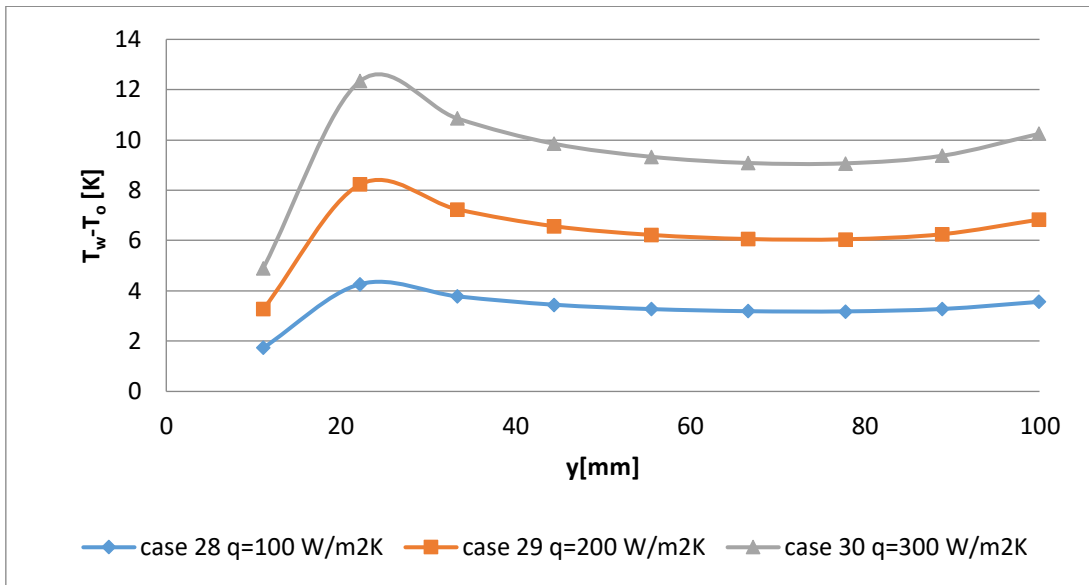


Figure 5.5. Temperature distribution for cavity with heat flux

As shown in Figure 5.6, increasing the heat flux causes decrease in the Nusselt number. This situation is also known from the theoretical formulation of the Nusselt number. With examining graphic 5.5 and 5.6 it is calculated that doubling the flux value, causes decreases in the temperature difference 1.5 times and rise the mean Nusselt number 1.15 times.

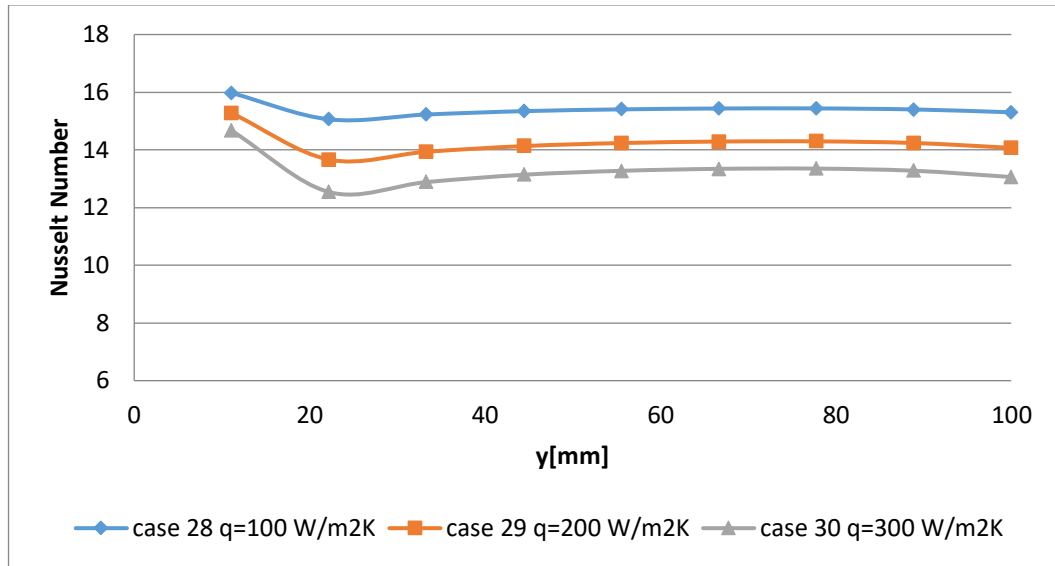
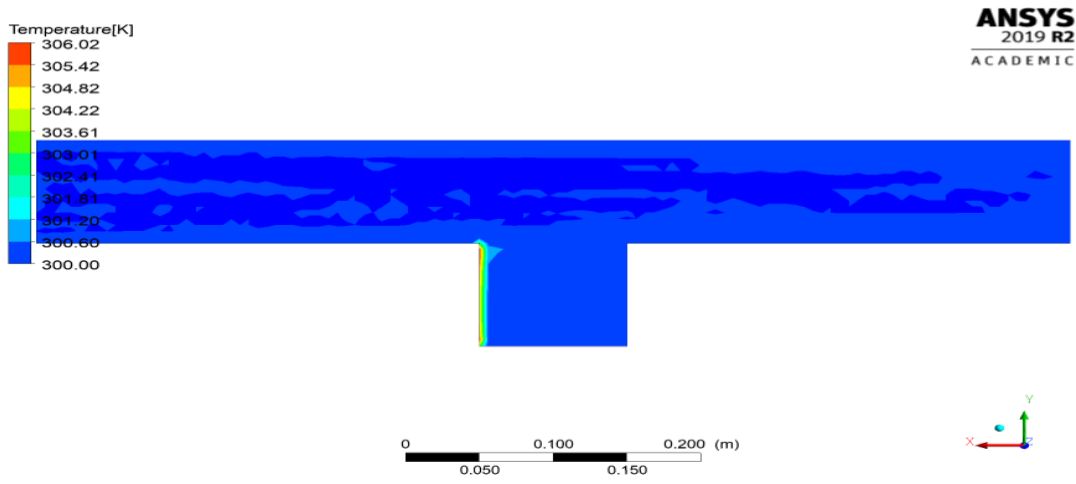
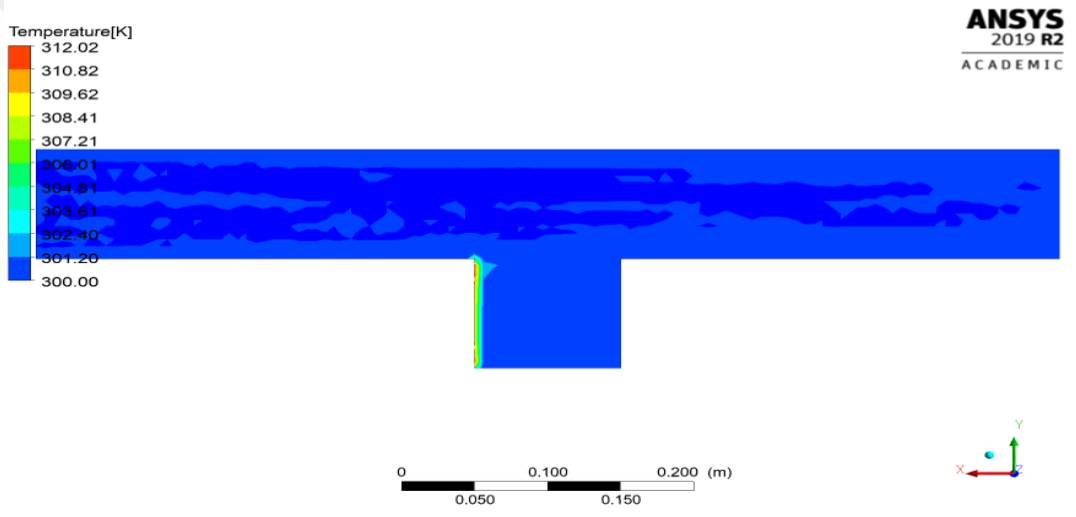


Figure 5.6. Averaged Nu number for a cavity with Heat Flux

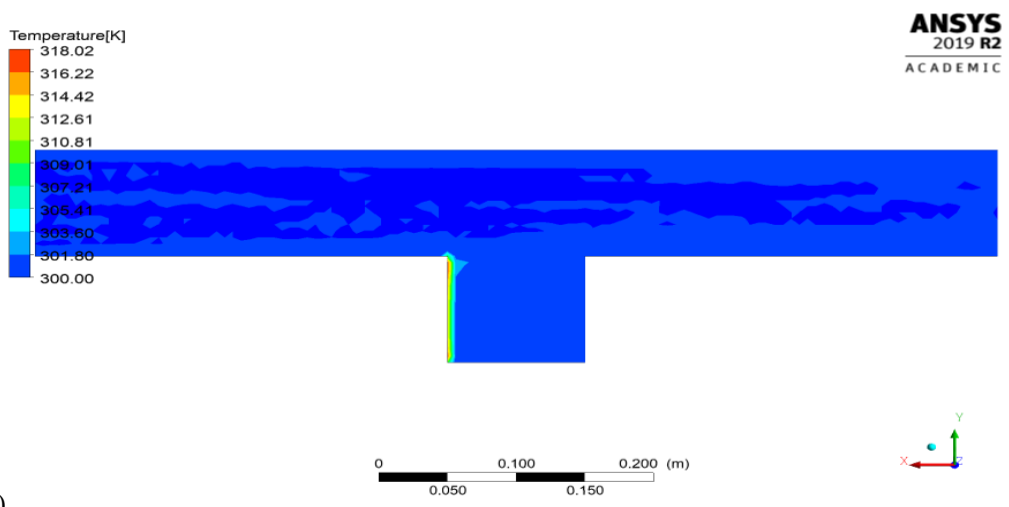
In Figure 5.7, temperature contours are given for different heat flux values. Since the geometry is kept constant, flow topology was observed in all cases in the cavity region. Also, since the number of Reynolds was constant, velocity distribution is similar. As the only change is the heat flux value, maximum temperature values are different. When the heat flux increases maximum temperature value also increases.



(a)



(b)



(c)

Figure 5.7 Temperature contour for (a)100W/m² (b) 200 W/m² (c)300 W/m²

5.3. Effect of Heated Wall Position on Heat Transfer Characteristics

Figure 5.8 presents the schematic view of the basing heating modes. In the first case, the right wall is heated which is called as assisting flow. In the second case left wall is heated and called as opposing flow, and the last case bottom wall is heated. Heating one wall with uniform heat flux and keeping other walls in constant temperature causes an interaction between a buoyancy induced flow and a forced flow.

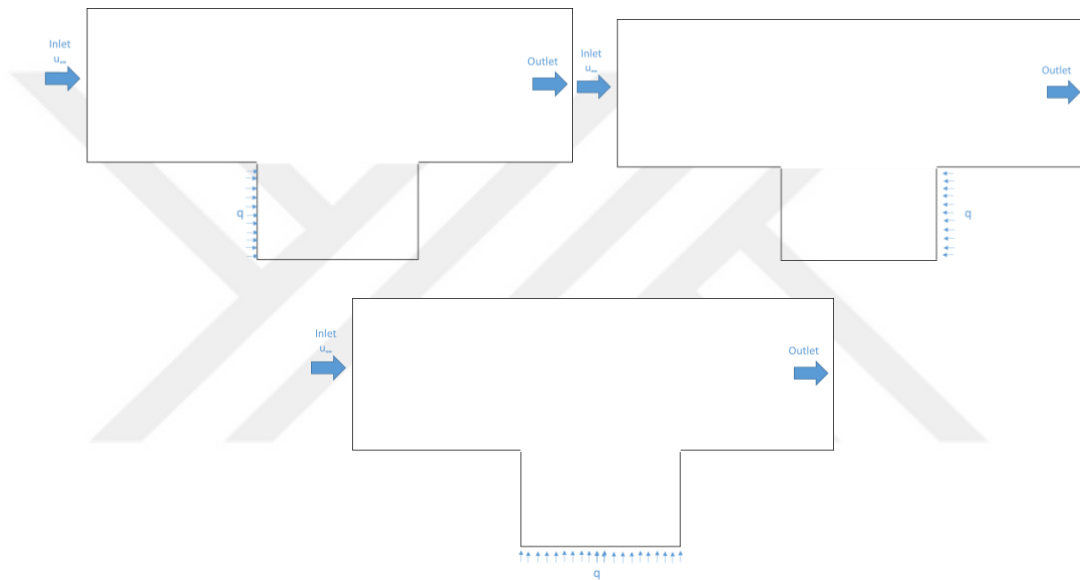


Figure 5.8. Schematic view of the (a) assisting flow (b) opposing flow
(c) bottom heated flow

In Figure 5.9 and 5.10, temperature difference and Nusselt number distribution are presented for different heating location cases. Due to the results, best heat transfer enhancement is achieved when opposing wall is heated. As incoming air hits to the warm air which moves in the spanwise direction and mixing occur efficiently. When assisting wall is heated, maximum temperature difference and minimum Nusselt number is observed.

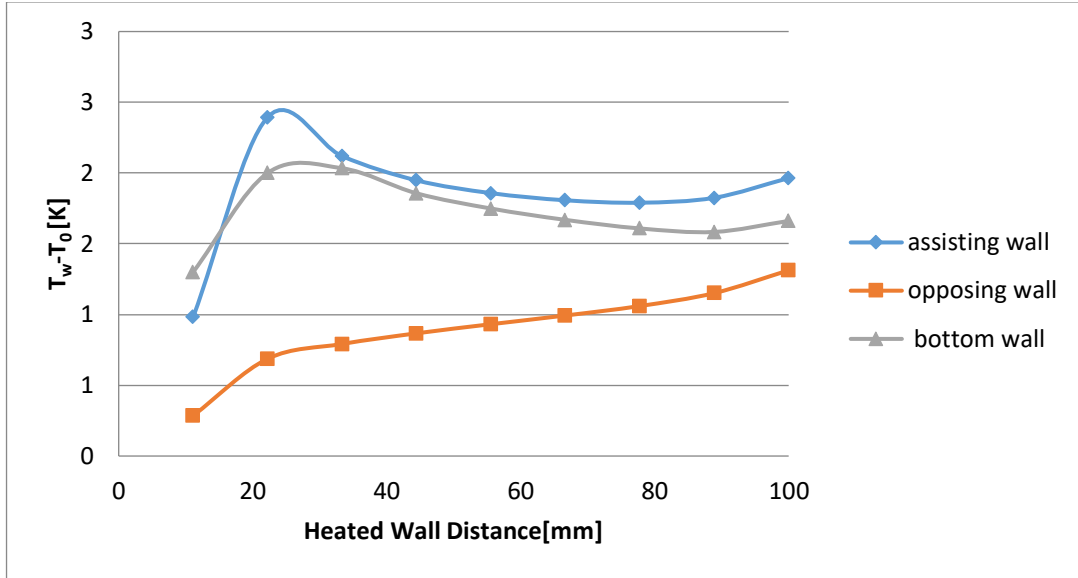


Figure 5.9. Temperature distribution for different heating locations

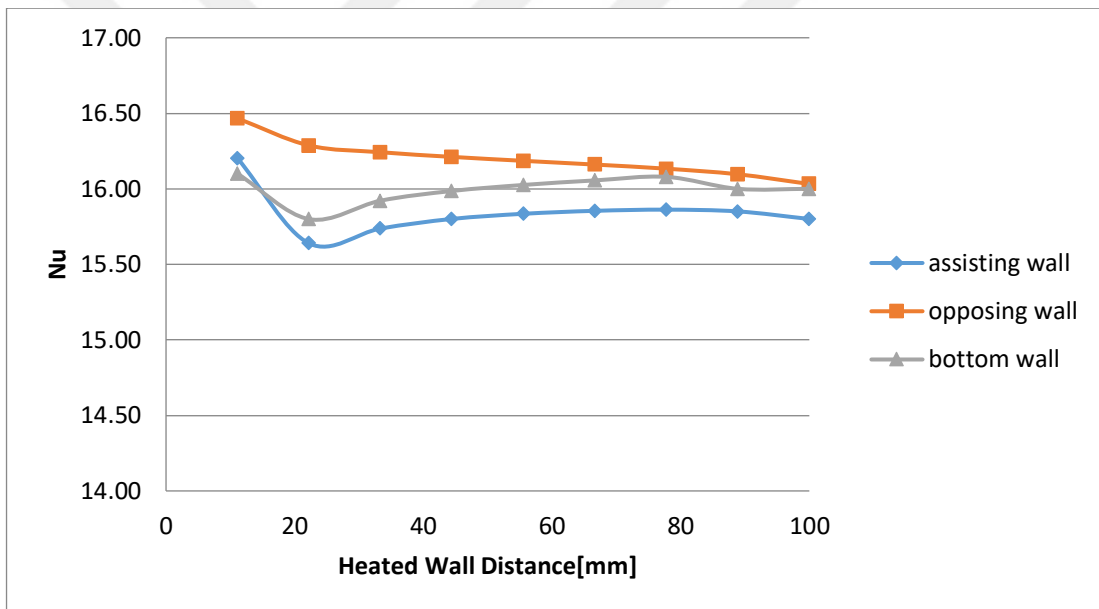


Figure 5.10. Nusselt number distribution for different heating locations

In Figure 5.11, temperature contour, and velocity vector for assisting flow, opposing flow and bottom heated flow are shown. In the opposing wall condition, cold fluid penetrates with hot fluid efficiently and temperature values decrease in the cavity zone. In the bottom wall heated configuration, like opposing wall case temperature values decreases in the cavity area. However when assisting wall is heated, temperature values are higher than the other cases. It is assumed that

buoyancy effect is smaller than mechanical effect of induced flow in bottom wall heated case.

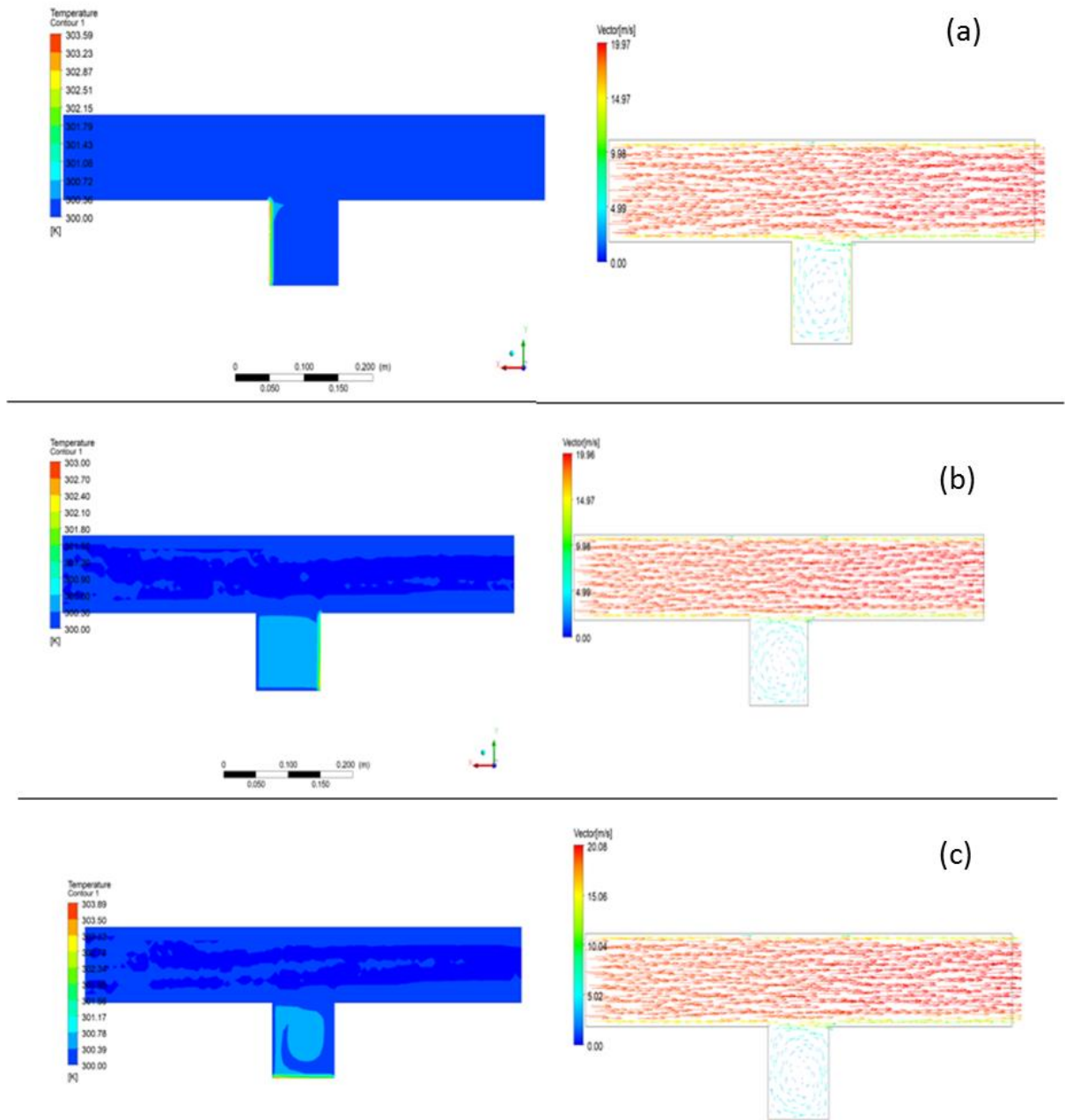


Figure 5.11. Temperature contour and velocity vector for (a) assisting flow (b) opposing flow (c) bottom heated flow

5.4. Effect of Richardson Number on Heat Transfer Characteristics

Ri number expresses the rate of the buoyancy term to the flow shear term as it is dedicated below.

$$Ri_H = Gr_H / Re_H^2 \quad (5.1)$$

The physical meaning of the Richardson number is the ratio of the buoyancy term to the flow shear term. To investigate the effect of Richardson number it is varied between $0.1 < Ri < 10$ for case 3. When $Ri < 1$, a small recirculating cell is observed in the cavity region. Conduction is dominant in the cavity zone. As the buoyancy effect is small then the mechanical effect of the induced flow Nusselt number is small in the smallest Richardson number. When Richardson number is larger than the unity, buoyancy effect is dominant and Nusselt number increases. In the cavity zone, circulation increases and recirculating cell gets larger.

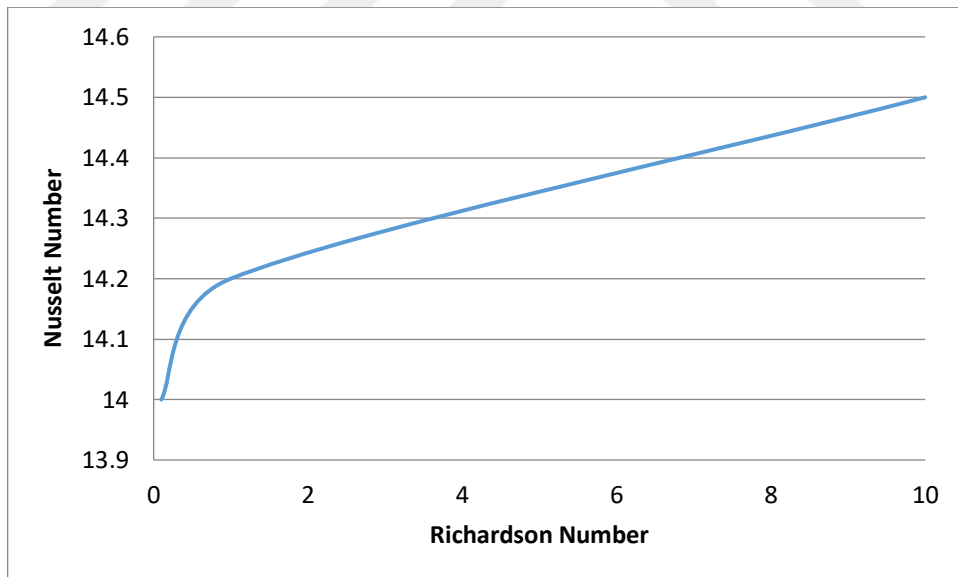


Figure 5.12. Richardson number effect in the mixed convection of open cavity

In conclusion, it is found that the Richardson number has a direct effect on heat transfer. When Richardson number is smaller than unity as buoyancy effects are recessive, incoming air can not mix efficiently with warm air. On the other hand; when Richardson number is larger than one, buoyancy effects are dominant. The hydrodynamic boundary layer is developed, circulation rises which cause turbulence and therefore Nusselt number increases.



CHAPTER 6

CONCLUSION

In this study, combined forced and natural convection heat transfer and fluid flow are examined in an open cavity. The effects of cavity geometries like cavity depth, cavity length, on heat transfer rate are investigated. As a flow parameter, Reynolds number, heat flux, Richardson number effects are examined.

The cavity left wall is heated with constant heat flux, while other walls are kept at the adiabatic condition. The working fluid is assumed as air with $Pr=0.71$. For numerical analysis FLUENT Software is used in order to solve incompressible, two-dimensional, steady-state flow. For momentum and energy equations second-order upwind scheme is used. Length to depth ratio and height to depth ratio of the cavity is varied between $0.25 < L/H < 2$, $0.25 < D/H < 3$, respectively. Reynolds number is changed between $24000 < Re < 96000$. In order to observe the effect of This study yields to following conclusions:

- When the Reynolds number is increased, the circulation is observed in the cavity, which causes higher Nusselt numbers.
- Decreasing D/H ratio which means increasing the cavity depth rises the temperature difference. Increasing the cavity depth causes lower heat transfer coefficient and heat transfer characteristics.
- When $D/H < 1$, the Nusselt number is higher when it is compared with the cases $D/H > 1$. As it is given in Figure 6.1, in the cases that cavity depth is smaller than cavity length vortex structure fills the cavity zone which increases the turbulence and causes heat transfer enhancement. On the other hand, when cavity depth is larger than the cavity height, vortex structures cannot reach to the cavity bottom and mixing of the incoming air, and warm air cannot be formed enough which results with lower Nusselt number.

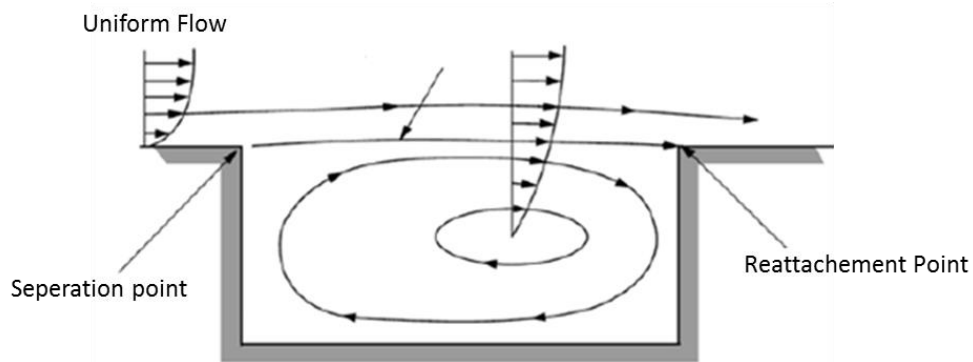


Figure 6.1. Schematic view of an open cavity with $D/H < 1$

- Increasing the cavity length increases the turbulent effect which causes heat transfer enhancement with higher Nusselt number values. In the higher L/D ratio cavity configurations, secondary vortices are observed in the cavity zone which results with higher heat transfer coefficient and Nusselt number (Figure 6.2). When cavity length is smaller than cavity depth, incoming flow cannot enter to the cavity region, therefore, temperature difference rises.

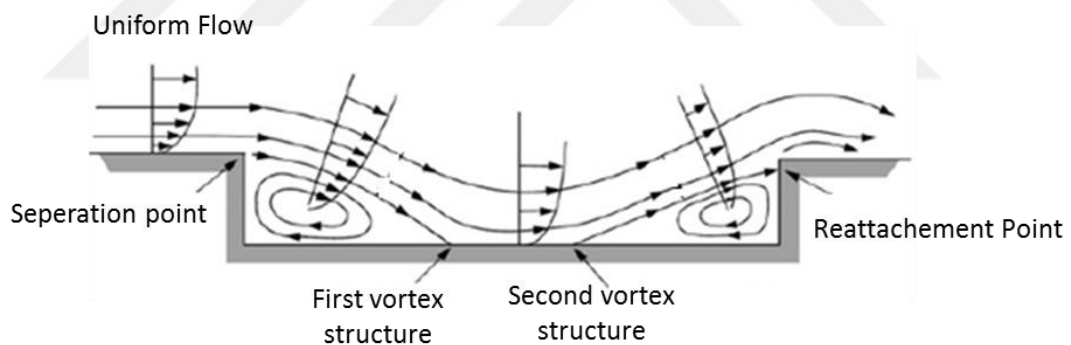


Figure 6.2. Schematic view of an open cavity with $L/D > 1$

- Different wall heating modes creates differences in Nusselt number distribution. Opposing wall heating is the best choice to achieve heat transfer enhancement.
- Richardson number has a direct effect on heat transfer. When $Ri < 1$ buoyancy effects are negligible when $Ri > 1$ buoyancy effects are dominant. Increasing the Richardson number rises the Nusselt number.

As a further study, it is recommended that experimental study can be performed and results can be compared with the numerical results. Also to observe the inclination effect effectively, analysis can be performed for constant wall length.



REFERENCES

1. N. Brown, F. Lai, Correlations for combined heat and mass transfer from an open cavity in a horizontal channel, *Int. Commun. Heat Mass*. 32 (2005) 1000–1008.
2. O. Manca, S. Nardini, K. Vafai, Experimental investigation of mixed convection in a channel with an open cavity, *Exp. Heat Transf.* 19 (2006) 53–68.
3. E. Papanicolaou, Y. Jaluria, Mixed convection from an isolated heat source in a rectangular enclosure, *Numer. Heat Transfer A* 4 (18) (1991) 427-461.
4. E. Papanicolaou, Y. Jaluria, Transition to a periodic regime in mixed convection in a square cavity, *J. Fluid Mech.* 239 (1992) 489-509.
5. E. Papanicolaou, Y. Jaluria, Mixed convection from a localized heat source in a cavity with conducting walls: a numerical study, *Numer. Heat Transfer A* 4 (23) (1993) 463-484.
6. R. Showole, J. Tarasuk, Experimental and numerical studies of natural convection with flow separation in upward-facing inclined open cavities, *ASME J. Heat Transfer* 115 (1993) 592–605.
7. O. Polat, E. Bilgen, Laminar natural convection in inclined open shallow cavities, *Int. J. Therm. Sci.* 41 (2002) 360–368.
8. E. Bilgen, H. Oztop, Natural convection heat transfer in partially open inclined square cavities, *Int. J. Heat Mass Transf.* 48 (2005) 1470–1479.
9. A. Piña-Ortiz, J. Hinojosa, V. Maytorena, Test of turbulence models for natural convection in an open cubic tilted cavity, *Int. Commun. Heat Mass* 57 (2014) 264–273.
10. Z. Mehrez, A. Cefsi, A. Beghith, P. Quéré, The entropy generation analysis in the mixed convective assisting flow of Cu-water nanofluid in an inclined open cavity, *Adv. Powder Technol.* 26 (2015) 1442–1451.
11. Manca, O., Nardini, S., Vafai, S., Experimental Investigation of Mixed Convection in a Channel With an Open Cavity, *Experimental Heat Transfer*, vol:19, pp:53-68,2006
12. Cardenas, V., Trevino, C., Rosas, I.Y., Martinez-Suastegui, L., Experimental study of buoyancy and inclination effects on transient mixed convection heat transfer in a channel with two symmetric open cubic cavities with prescribed heat flux, *International Journal of Thermal Sciences*, vol: 140, pp: 71-86,2019
13. A. Elatar, K. Siddiqui, The influence of bottom wall heating on the mean and turbulent flow behavior in the near-wall region during mixed convection, *Int. J. Therm. Sci.* 77 (2014) 233-243.
14. A. Elatar, K. Siddiqui, The characteristics of coherent structures in low Reynolds number mixed convection flows, *Fluid Dyn. Res.* 47 (2015)

15. A. Elatar, K. Siddiqui, Flow development during low Reynolds number mixed convection, *Int. J. Therm. Sci.* 90 (2015) 351-369.
16. J. Wang, J. Li, J. D. Jackson, A study of the influence of buoyancy on turbulent flow in a vertical plane passage, *Int. J. Heat. Fluid Flow.* 25 (2004) 420-430.
17. M. Kühn, K. Ehrenfried, J. Bosbach, C. Wagner, Large-scale tomographic PIV in forced and mixed convection using a parallel SMART version, *Exp. Fluids* 53 (2012) 91-103.
18. Y. Liu, E. A. Groll, K. Yazawa, O. Kurtulus, Energy-saving performance and economics of CO₂ and NH₃ heat pumps with simultaneous cooling and heating applications in food processing: case studies, *Int. J. Refrig* 73 (2017) 111-124.
19. O. Shishkina, C. Wagner, Highly-resolved numerical simulations of high Rayleigh and Reynolds number indoor ventilation in a generic room, in: A. Dillmann, G. Heller, E. Kramer, H.-P. Kreplin, W. Nitsche, U. Rist (Eds.), *New Results Numer. Exp. Fluid Mech. IX Contrib. To 18th STAB/DGLR Symp*, Springer International Publishing, Cham, 2014, pp. 303-311.
20. G. Yang, J. Y. Wu, Analysis of temperature uniformity in a spacecraft thermal-cycling test system based on wavelet transform and multiple regression, *J. Shanghai Jiaotong Univ.* 48 (2014) 1346-1350.
21. L. Zhang, Y. Zhang, B. Zhao, W. Ma, Y. Zhou, G. H. Su, et al., COPRA: a large scale experiment on natural convection heat transfer in corium pools with internal heating, *Prog. Nucl. Energy* 86 (2016) 132-140.
22. J. J. Niemela, L. Skrbek, K. R. Sreenivasan, R. J. Donnelly, Turbulent convection at very high Rayleigh numbers, *Nature* 404 (2000) 439.
23. S. Pirozzoli, M. Bernardini, R. Verzicco, P. Orlandi, Mixed convection in turbulent channels with unstable stratification, *J. Fluid Mech.* (2016) 1-30.
24. L. Zhang, Y. Zhang, B. Zhao, W. Ma, Y. Zhou, G. H. Su, et al., COPRA: a large scale experiment on natural convection heat transfer in corium pools with internal heating, *Prog. Nucl. Energy* 86 (2016) 132-140.
25. G. Evans, R. Greif, D. Siebers, S. Tieszen, Turbulent mixed convection from a large, high temperature, vertical flat surface, *Int. J. Heat. Fluid Flow.* 26 (2005) 1-11.
26. Burgos, J., Cuesta, I., Saluna, C., Numerical study of laminar mixed convection in a square open cavity, *International Journal of Heat and Mass Transfer*, Vol: 99, pp: 599-612, 2016.
27. Aminossadati, S.M., Ghasemi ,B., A numerical study of mixed convection in a horizontal channel with a discrete heat source in an open cavity, *European Journal of Mechanics-B/Fluids*, vol: 28, pp:590-598,2009.

28. Rajarathinam, M., Nithyadevi, N., Chamka, A.J., Heat transfer enhancement of mixed convection in an inclined porous cavity using Cu-water nanofluid, *Advanced Powder Technology*, Vol: 29, pp: 590-605,2018.
29. Koufi, L., Zohir, Y., Hasanne, N., Numerical investigation of turbulent double-diffusive mixed convection in a slot ventilated enclosure with supply airflow ports, *23 ème Congrès Français de Mécanique*.
30. Timuralp, Ç., Altaç, Z., Investigation of Combined Heat Transfer and Laminar Fluid Flow in Two and Three Dimensional Ducts with an Open Cavity, *Journal of Thermal Science and Technology*, vol: 37, pp:33-47,2017.
31. Fluent's User Manual. Fluent Ver. 6.3.26. Fluent Inc.
32. Launder, B.E., Spalding, D.B., *Mathematical Models of Turbulence*, Academic Press, 25(4), 169-172, 1972
33. Kolmogorov, A.N., Equations of Turbulent Motion of an Incompressible Fluid, *Izvestia Academy of Sciences, USSR; Physics*, 6, 56-58, 1942.
34. O. Manca, S. Nardini, K. Vafai, K. Khanafer, Effect of Heated Wall Position on Mixed Convection in A Channel with an Open Cavity *Num. Heat Transf. Part A*,43,pp: 259-282 ,2003.